Assessment of CFD Performance in Simulations of an Idealized Medical Device - Results of FDA's First Computational Interlaboratory Study

Sandy F.C. Stewart[1], Eric G. Paterson[2], Greg W. Burgreen[3], Prasanna Hariharan[1], Matthew Giarra[4], Varun Reddy[2], Steven W. Day[4], Keefe B. Manning[2], Steven Deutsch[2], Michael R. Berman[1], Matthew R. Myers[1], and Richard A. Malinauskas[1]

[1]*Food & Drug Administration, Silver Spring, MD USA*
[2]*Pennsylvania State University, University Park, PA USA*
[3]*Mississippi State University, Starkville, MS USA*
[4]*Rochester Institute of Technology, Rochester NY USA*

Address for Correspondence: Sandy F.C. Stewart, Office of Science and Engineering Laboratories, Food and Drug Administration, 10903 New Hampshire Ave., Bldg 62, Rm 2210, Silver Spring MD 20993. Tel: 301-796-2518. Fax: 301-796-9932. E-mail: sandy.stewart@fda.hhs.gov

Abstract

While computational fluid dynamics (CFD) is commonly used for medical device development, its usefulness for demonstrating device safety has not been proven. Reliable standardized methods for this specialized need are lacking and are inhibiting the use of computational methods in the regulatory review of medical devices. To meet this need, participants from academia, industry, and the U.S. Food & Drug Administration recently completed a computational interlaboratory study to determine the suitability and methodology for simulating fluid flow in an idealized medical device. A technical working committee designed the study, defined the model geometry and flow conditions, and identified comparison metrics. The model geometry was a 0.012 m diameter cylindrical nozzle with a conical collector and sudden expansion on either side of a 0.04 m long, 0.004 m diameter throat, which is able to cause hemolysis under certain flow conditions. Open invitations to participate in the study were extended through professional societies and organizations. Twenty-eight groups from around the world submitted simulation results for five flow rates, spanning laminar, transitional, and turbulent flows. Concurrently, three laboratories generated experimental validation data on geometrically-similar physical models using particle image velocimetry. The simulations showed considerable variation from each other and from experiment. One main source of error involved turbulence model underestimations of the centerline velocities in the inlet and throat regions, because the flow was laminar in these regions. Turbulence models were also unable to accurately predict velocities and shear stresses in the recirculation zones downstream of the sudden expansion. The wide variety in results suggest that CFD studies used to assess safety in medical device submissions to the FDA require careful experimental validation. Better transitional models are needed, as many medical devices operate in the transitional regime. It is

imperative that the community undertake and publish quality validation cases of biofluid dynamics and blood damage that include complications such as pulsatility, secondary flows, and short and/or curved inlets and outlets. The results of this interlaboratory study will be available in a benchmark database to help develop improved modeling techniques, and consensus standards and guidelines for using CFD in the evaluation of medical devices.

Keywords: *computational fluid dynamics, experimental validation, medical devices, blood damage*

Introduction

Computational fluid dynamics (CFD) is a powerful tool used in many industries to develop new products. Combined with computer aided design, the technology can be employed in virtual prototyping so as to cut costs and speed development by eliminating the expensive and time-consuming manufacture and bench testing of interim designs. In the medical device industry, CFD has been used to develop and/or analyze ventricular assist devices,[2,18,32] prosthetic heart valves,[4,10,21] stents,[16,24] blood filters,[7] and peripheral hemodialysis cannulas.[3] CFD is equally useful in the design of minor changes to medical devices.[28,31] It has also been called upon to investigate problems with commercial devices.[5,14]

Blood flowing through medical devices may be subject to hemolysis and thrombosis. The deleterious effects of high shear stresses on blood have been known for many years.[27,30] For hemolysis, this relationship is often expressed as a shear stress/exposure time relationship, which shows that high shear stresses can only be tolerated for short times before blood damage occurs, while low shear stresses can be tolerated for longer times.[36] This relationship has been quantified empirically,[11] and, along with other methods,[13] is now being used in conjunction with CFD to perform hemolysis predictions in medical devices.[1,9,12,25,32,35] Computational methods for predicting platelet activation[4,26] and thrombosis[6,29,33,34] are also active areas of research.

Such computations are already being used both in the developmental stage and in predicting safety of the final design. However, whether CFD can reliably and consistently demonstrate product safety remains open. Using CFD to demonstrate safety for regulatory purposes has more stringent requirements than using it to develop the device. In particular, the shear stress field and time exposure metrics need to be more accurate and better characterized when using CFD for safety assessments than for device development alone (which can rely more

on relative measures). Furthermore, methods to predict hemolysis and thrombosis are in their infancy, and comprehensive theoretical understanding and experimental validation of blood-damage models is lacking. For both design and regulatory uses, experimental validation plays an essential role.

The goal of this study was to assess the current state of the art in CFD modeling with respect to predicting fluid dynamics in an idealized medical device model. To this end, we solicited from the worldwide CFD community CFD simulations and blood damage predictions in the model we designed. The specific aims of our study were to: 1) develop a suitable benchmark model for the interlaboratory study (as well as for future research and standards development); 2) evaluate and compare each participant's CFD simulations against quantitative flow visualization experiments carried out in three independent laboratories; and 3) extract needed input for the development of standards and guidelines for industry and FDA reviewers who employ or consider CFD in premarket device applications and postmarket investigations of device problems. This paper describes the fluid dynamics results only. A future report will address the blood damage aspects.

Methods

Nozzle Model

The interlaboratory study considered a simplified, idealized medical device consisting of a small nozzle (Figure 1a). The nozzle shares characteristics of blood-carrying medical devices, such as blood tubing, hemodialysis sets, catheters, cannulas, syringes, and hypodermic needles. Geometrically, the model includes a radial step, sharp edges, and a cross-sectional stenosis that combine to induce shear stresses related to reported problems in these devices, such as hemolysis due to tubing kinks and molding flash. The device was designed to include accelerating flow,

decelerating flow, variations in shear stress and velocities, and recirculating flow, all of which may be related to blood damage in medical devices. The axisymmetric nozzle incorporates a 0.04 m long stenotic throat with a 20° connecting cone on one end of the throat, and a step change in diameter on the other end. With the flow going from left to right as in Figure 1a, the nozzle models a conical collector and a sudden expansion. With flow going from right to left, the nozzle models a sudden contraction and a conical diffuser. Similar nozzles have been the subject of previous computational, experimental, and blood damage experiments.[6,17,19,20,29]

Simulation Conditions

Participants were asked to perform a series of simulations for both flow orientations. The model oriented with flow entering the conical collector and exiting through the sudden expansion was denoted the "Sudden Expansion." The model oriented with flow in the opposite direction was denoted the "Conical Diffuser." This report focuses on the Sudden Expansion only; the Conical Diffuser results will be discussed in a future report. Five simulations were run for each orientation. The volumetric flow rates and corresponding throat and inlet Reynolds numbers are given in Table 1. The flow rates are characterized by the throat Reynolds number, Re_t. The flow rates were chosen to cover the laminar, transient, and turbulent regimes. The fluid was specified to be Newtonian, with a fluid density and dynamic viscosity of 1056 kg/m^3 (1.056 g/cm^3) and 0.0035 $N \cdot s/m^2$ (3.5 cP), respectively.

Participants were free to choose the solver, mesh density, element shape, inlet/outlet lengths, inlet/outlet boundary conditions, turbulence model (if needed), and all other parameters of their simulations, according to their individual preference and experience. Participants were also asked to perform a grid refinement study for the Sudden Expansion at $Re_t = 5000$. Participants were free to perform simulations on as many grids as they thought necessary, and

the production grid used for the other flow rates could be any one of the grids. For comparison and analysis purposes, participants were requested to provide simulation data along the model centerline, at various radial cuts (defined in Figure 1b), and along the wall. Flow variables requested along the centerline and radial cuts were the velocity components, pressures (centerline only), shear stresses, and Reynolds stresses (if a turbulent model was used). Flow variables requested along the nozzle wall were the wall shear stress and wall pressure, the latter intended to be compared to data from an experimental pressure tap model. Participants were also invited to provide an index of hemolysis for each simulation (normalized to the value at Re_t = 3500 in the Conical Diffuser); this data will be discussed in a future report. A total of 28 groups submitted the results of their simulations, which included three sets of data from authors of this paper. Full documentation for the nozzle study may be found at https://fdacfd.nci.nih.gov/.

Experimental Validation

The particle image velocimetry (PIV) methods and error analysis have been reported in detail previously.[15] Briefly, identical acrylic nozzle models were fabricated using a numerically-controlled milling machine from computer-aided design plans. Following fabrication, the models were carefully polished inside and out for optical transparency. Model accuracy was maintained within 1% of the specified dimensions. Surface roughness was measured to be $<5.0 \times 10^{-7}$ m (0.50 μm). The radius of curvature of the sharp corner at the sudden expansion, where the inner diameter (I.D.) increases abruptly from 0.004 m to 0.012 m, was measured to be $<2.5 \times 10^{-5}$ m (25 μm). The acrylic models were 0.25 m long. Acrylic extender tubes with a constant 0.012 m I.D. were glued onto either end of the nozzle sections to extend the possible range of flow visualization. Additional extenders of stainless steel with the same I.D. were then glued to the acrylic models to allow for fully-developed velocity profile at the inlet.

The models were connected to a steady flow loop with flow driven by a centrifugal pump.[15] The working fluid was a solution of water, glycerin, and sodium iodide (NaI), with the refractive index of the fluid (1.489) matched to that of the acrylic to avoid optical distortion by the curved inner surfaces. The working fluid temperature was kept constant to within ±0.5 °C, as small changes in temperature caused errors due to changes in viscosity.[15] Reservoirs and flow straighteners at the inlet helped provide the inlet flow with a symmetric velocity profile. Flow rates were adjusted to match Re_t in Table 1 because the working fluid viscosity and density were higher than that specified for the CFD simulations (due to the dissolved NaI).

The working fluid was seeded with 10 μm hollow glass spheres and illuminated in a plane containing the nozzle centerline by a dual pulse laser spread into a light sheet approximately 0.5 mm thick. The illuminated flow was then photographed with laser pulses synchronized to the video. Thus pairs of images could be taken with a user-variable increment of time between. The two images were then subjected to a correlation analysis which provided two-dimensional velocity data in the image plane. Shear rates were calculated from the velocity field. Reynolds stresses were calculated using the statistics from 500-2500 pairs of images at the same flow rate and position. Velocities and stresses were then normalized by the working fluid density and viscosity to compare to the CFD results.[15]

Pressures were also measured in a separate acrylic model manufactured with wall pressure taps along the length of the model. This model was tested in the same flow loops used for PIV at the three laboratories. A water/glycerin solution was used with the flow rates adjusted to give the same Re_t as in the CFD simulations and PIV experiments. Experimental uncertainty analysis of bias and precision errors, including facility bias of experiments conducted at the three laboratories, are discussed in a previous report.[15]

Data Analysis

Once all the participants had submitted their simulations, the CFD and experimental data was blinded by replacing the author name and institution with a three digit code. A Python script was developed to resolve a variety of typographical and formatting errors in the data files. A data mining and analysis program written in CodeGear™ Delphi® 2009 was used to aggregate selected blinded data, provide x-y plots of the CFD and experimental data and to calculate a validation velocity metric. The data could be plotted with reference to any of the data found in the file headers (such as the turbulence model used). The blinded and error-corrected data detailed in this paper and data mining and analysis program are available for download at https://fdacfd.nci.nih.gov/.

Conservation of Mass Metric

Simulations should obey fundamental conservation laws such as the conservation of mass. For incompressible flow and this particular nozzle geometry, conservation of mass can be locally evaluated at each of the axial stations shown in Figure 1b by integrating the axial velocities along the radius for both the experimental and simulated data. Since blood is an incompressible fluid, the volumetric flow rate should remain constant as a function of axial position. The conservation of mass error metric as a function of axial position z was defined as:

$$E_Q = \frac{Q_{CFD} - Q_{theory}}{Q_{theory}} \times 100\% \quad (1)$$

where Q_{CFD} = the volumetric flow rate computed from the CFD axial velocity profiles, and Q_{theory} = theoretical volumetric flow rate calculated from the throat Reynolds number. For axisymmetric meshes, Q_{CFD} was calculated from zero radius to the outer radius of the nozzle, along the twelve axial velocity profiles. For 3D meshes, Q_{CFD} was calculated across the diameter. The radius was dependent on location (inlet, outlet, throat, or cone). A simple

rectangle rule in radial coordinates was used for the numerical integration.

Validation Metrics

A generic validation metric E was defined to quantify the goodness of fit between a simulation and the averaged experimental measurements:[22,23]

$$E = \frac{1}{n}\sum_{i=1}^{n}\left|\frac{\overline{u}_{e,i} - u_{c,i}}{\overline{u}_{e,i}}\right|, \tag{2}$$

where E = validation metric, $\overline{u}_{e,i}$ = average of the experimental velocity data at one discrete point i along the radial cuts, $u_{c,i}$ = CFD data at the same point i, and n = number of discrete points. E is a non-negative number with the value of 0.0 indicating exact prediction by CFD of experiment. Only axial velocities were used in the error analysis because radial velocities were difficult to measure accurately in the PIV experiments:[15] radial velocities were low, and thus required relatively long times between image pairs, but, in that interval, particles typically moved out of the image frame due to the higher axial velocities.

Two specific validation metrics were employed in our error analysis. First, a global validation metric E_g was computed by using axial velocity data points along all the radial cuts shown in Figure 1b. Secondly, local validation metrics $E_z(z)$ were also computed using data along each of the twelve radial cuts taken separately, to evaluate the performance of the simulations as a function of axial position in the nozzle. Due to the lack of precise radial alignment among the PIV and CFD data, velocities were linearly interpolated between neighboring points at a pre-defined set of radii.

Results

Conservation of Mass Errors

The CFD predicted and experimental volumetric flow rates for Re_t = 3500 are plotted as a

function of axial position in Figure 2, with simulations having absolute flow rate errors $|E_Q| \leq$ 10% shown in Figure 2a, with the remainder, having $|E_Q| >$ 10%, shown in Figure 2b. Some of the simulations demonstrated unexpectedly large variations from the theoretical value. Unresolved errors in data formatting may have been responsible for some of the variation; however, several simulations simply appeared to not conserve mass over the entire solution domain. From 9 to 13 entries (depending on Re_t) had absolute flow rate errors $|E_Q| >$ 10%. Most of the k-omega/shear stress transport (SST) models appeared to do better in this regard, with most having $|E_Q| \leq$ 10% (Figure 2a). In contrast, most of the k-epsilon (KE) models did worse (Figure 2a). Because this is such a fundamental problem, simulations with any $|E_Q| >$ 10% were omitted from the remaining figures for clarity. We note that the experimental flow rates also contained non-trivial errors ($|E_Q|$ in a few cases > 10%), due to the difficulty in measuring velocities accurately at the wall, especially in recirculation zones downstream of the sudden expansion where velocities near the wall were low.[15]

Axial Velocity Along Centerline

The simulation results are compared to the experimental mean ± 95% confidence interval ($CI_{95\%}$) in Figure 3. At Re_t=500 (inlet Reynolds number = 167, Table 1), the flow was observed to be fully laminar in the PIV experiments. This includes the jet issuing from the sudden expansion,[15] a feature reported in previous studies.[8] Despite this, over half of the simulations (15/28) were performed using a turbulent model of some type (Table 2). Most of the laminar simulations matched the experiments within $CI_{95\%}$ of the experimental means at most of the axial points. The laminar simulation where the jet velocity decreased quickly had a short outlet tube length (0.080 m); it was also one of the few axisymmetric triangular meshes used. As for the

turbulent simulations, one of the SST models and one of the k-omega (KO) models were also able to match the experimental centerline velocity within $CI_{95\%}$ at most points. This agreement represents an unknown but fortuitous combination of factors since a turbulence model should not be employed at $Re_t = 500$. In another KO simulation (not shown because $E_q > 10\%$), the jet broke down much too soon, and showed blunting of the velocity profile upstream of the sudden expansion. This latter KO model was a transient simulation, while the former was steady flow. Turbulence intensity boundary conditions were not provided in either case but differences here also may have played a role. Otherwise both KO simulations were similar: both were 3D, were performed with the same code, both used the same element shape, and almost the same element size. The remaining simulations using turbulence models did not match experimental data downstream of the sudden expansion, with the KE model performing the least well. This is not surprising, because the KE model was developed for high Reynolds numbers and would be expected to be "tuned" for higher rates of turbulent dissipation than the KO and SST models. One reason that participants chose a turbulent model for this Re_t may have been the belief that jets issuing from a sudden expansion are turbulent. The interface between the jet and recirculation zone represents a genuine instability, but we observed no visible breakdown at $Re_t = 500$ in our experiments. Clearly, at this low Re_t, simple turbulence models should not be used.

At Re_t=2000, the flow downstream of the sudden expansion was observed in the experiments to be transitional, with large scale vortices filling the recirculation zones. Furthermore, the experimental jet breakdown point varied among the three laboratories, which was attributed to a 10% higher flow rate with a corresponding higher Re_t that caused premature jet breakdown in two of the three laboratories.[15] Experimental variations were also traced to minor differences in the settling chamber size and turbulence intensities upstream of the nozzle.[15]

These variations were responsible for the large experimental $CI_{95\%}$ at z = 0.060 and 0.080 m. Most of the simulations used turbulent models, divided between SST and k-epsilon (KE), with one KO model (Figure 3b). Two of the SST models used a transitional flow option, (arrows, Figure 3b). The three laminar models fit within $CI_{95\%}$ only up to the point of the jet breakdown. The turbulent simulation that fit best used was one of KO models; the other turbulence models were outside the experimental $CI_{95\%}$ at most of the downstream points. Overall, the KE models did the poorest job of matching experiment.

At Re_t=3500, turbulence downstream of the sudden expansion was observed in the experiments, with a reproducible jet breakdown point (Figure 3c), indicating a fully turbulent flow regime. At points downstream of the sudden expansion the experimental $CI_{95\%}$ were very tight. In general, the KE models caused the jet to break down too far upstream, as did the SST models (but not quite as badly). The KO model broke down too far downstream, while the laminar simulation did not match the centerline velocity at all well beyond the jet breakdown point. None of the simulations consistently matched the experimental centerline velocity within the 95% confidence interval downstream of the sudden expansion. These basic trends continued at Re_t=5000 (not shown) and 6500 (Figure 3d), with the differences between the experimental results and the KE results reducing slightly as Re_t increased. In general, the SST and the SA models performed well at Re_t=5000 and 6500; however, turbulence models consistently under-predicted the laminar axial velocities upstream of the nozzle throat by as much as 25-30%. At these higher throat Reynolds numbers, the KO models broke down farther downstream than experiment.

Pressure Variations

Wall pressures predicted by the simulations are compared to measurements obtained

from the wall tap model in Figure 4. All pressures are plotted relative to the pressure at z = 0.0 m (the location of the sudden expansion). Experiments were repeated three times at one lab only at Re_t = 3500. One set of experimental data was omitted at Re_t = 500 and at Re_t = 2000 due to significant measurement errors; thus n = 3, 3, 5, and 4 for Re_t = 500, 2000, 3500, and 6500, respectively. Experimental errors at the z = 0.0 m normalization point may partly explain the 100-250 N/m^2 (0.75-2.0 mmHg) offset at Re_t = 500. Errors were traced to not using differential pressure transducers in some of the experiments. Most of the CFD simulations that conserved mass predicted the pressures fairly well, regardless of turbulence model assumption. Little difference was observed between the computed wall pressures and centerline pressures (latter shown in inset figures in Figure 4) near the sudden expansion, indicating negligible radial pressure gradients.

Axial Velocity Profiles Along Radial Cuts

In the experiments the inlet flow was laminar at all Re_t except for two of the experiments at 6500, where the inlet Re at 2167 was in the transitional regime (Figure 5a). In contrast, participants employed a variety of inlet velocity profiles including plug, parabolic, and logarithmic (i.e., turbulent) profiles. Thus many of the simulations underestimated the axial velocities in the center of the inlet tube, but overestimated them near the wall. Experimentally, the flow profile was observed to become more blunt as it entered the conical collector as the average velocity increased (Figure 5b), and most of the simulations captured this behavior, regardless of inlet velocity profile. At Re_t = 500, the experimental flow profile in the throat became fully developed prior to the sudden expansion (Figure 5c), even though the theoretical entrance length from the downstream end of the conical diffuser (0.06*Re*D ~ 0.12 m) is longer than the throat length (0.04 m). Again, most of the simulations were able to capture this

behavior. Just downstream of the sudden expansion (Figure 5d), the KE models deviated substantially from the experiments. The one laminar model that performed poorly downstream of the sudden expansion used a moderately coarse triangular mesh, which is associated with high artificial dissipation. Overall, the laminar and SST models were able to capture the very low negative velocities within the recirculation zone. Further downstream (Figure 5e and f), the profiles from turbulent models departed further from experiment. Reverse flow in the recirculation zone was captured only by the laminar simulations and one each of the SST and the KO turbulence simulations.

At $Re_t = 2000$, differences in fluid properties (around 10%) among the three PIV labs, along with differences in inlet perturbations levels, were sufficient to cause substantial variations in the experimental reattachment lengths for the transitional flow case (Figure 3b). While the confidence intervals for the experimental axial velocities were small over most of the radial cuts (Figure 6a, b, c, d), there were substantial interlaboratory variations at z = 0.060 m (Figure 6e), and less so at z = 0.080 m (Figure 6f).

The inlet profiles from the CFD simulations at $Re_t = 2000$ departed more from experiment when turbulence models were used that assumed full turbulence everywhere, because the inlet flow was observed to be laminar (Figure 6a). Just downstream of the sudden expansion (Figure 6c), most of the laminar and SST models predicted the profile of the blunted jet and decrease in velocity with radius fairly well. The KO model had a more rounded profile near the nozzle axis that did not match experiment, while the KE models performed poorly over the entire radius. Only the laminar simulations captured the mean velocity profiles well 0.032 m downstream of the sudden expansion (Figure 6d). In contrast, at 0.080 m downstream (Figure 6f), only the turbulent models matched the mean velocity profiles of the experiments.

As would be expected, the instantaneous velocities observed in preliminary high speed videos (not shown) were much more complex than the mean velocities predicted by any of the CFD models would suggest. Flow in the recirculation zone was observed to be highly disorganized and three-dimensional, with large vortices filling the recirculation zone at irregular intervals that decayed rapidly. This illustrates that a simulation can match experimental data well in some respects but not others (e.g., mean vs. instantaneous velocities), and in some locations but not others (e.g., close to vs. farther from the sudden expansion). Comparisons of turbulence intensity or Reynolds stresses would be useful, but there was so little agreement in Reynolds stresses that we elected not to show them here.

At Re_t = 3500, the experimental inlet flows were observed to be laminar (Figure 7a). At Re_t = 6500 the inlet flow was measured as turbulent at only two of the three laboratories (Figure 8a), due to minor variations in flow rate at the inlet.[15] The equivalent inlet Reynolds number = 2167 (Table 1) is in the transitional regime at Re_t=6500, so that minor flow rate variations can have a substantial effect on the nature of the flow. Upstream of the sudden expansion (Figure 7 and Figure 8, panels b and c), the simulations did an adequate job of predicting experiment. Downstream of the sudden expansion, the simulations using turbulence models did not predict flow in the recirculation zones closely (Figure 7 and Figure 8, panels d and e). Only downstream of the reattachment point did the turbulent simulations adequately predict the velocity profile (panel f in Figure 7 and Figure 8).

Shear Stress Profiles

The shear stress magnitude, $|\tau|$, was defined in this study as:

$$|\tau| = 2.0\mu\sqrt{S_{ij}S_{ij}}\,, \tag{3}$$

where S_{ij} = components of strain-rate tensor, μ = dynamic viscosity, and repeated indices indicate

summation. Figure 9 shows $|\tau|$ for three radial cuts in the nozzle, for Re_t = 500. Most of the laminar and SST models performed well in the inlet (Figure 9a) and collector (Figure 9b) regions. Two of the three laminar simulations showed nonlinear $|\tau|$ profiles due to simulation choices such as a plug flow inlet boundary condition, and short inlet length. The highest laminar curve and lowest KE curve may have been contaminated with scaling errors, due to an error in the definition of shear rate in the original project documentation, later corrected in an update possibly not observed by all participants. The KE models showed nonlinear $|\tau|$ profiles corresponding to non-parabolic turbulent velocity profiles. Near the sudden expansion (Figure 9c and d), most of the simulations performed well. In the outlet sections (Figure 9e and f), many of the $|\tau|$ predictions were in error by 100% or more, directly related to errors in the predicted velocity profiles. Some of the laminar and SST models predicted $|\tau|$ fairly well, including the peak at the boundary between the jet and the recirculation zone and the nadir in the center of the recirculation zone.

At Re_t = 2000, only the laminar simulations and a few of the SST simulations were able to correctly predict $|\tau|$ in the inlet region (Figure 10a). Some of the SST models predicted nonlinear $|\tau|$ profiles (or had inlet boundary conditions that resulted in nonlinear profiles), possibly due to unreasonably high turbulence intensities applied as the inlet boundary condition. In the collector and throat, most of the models did a fair job near the centerline, but varied considerably nearer the wall (Figure 10b and c). Many of the KE models performed poorly near the centerline. There were also errors in the experiment due to the difficulty in performing PIV near the wall.[15] At the sudden expansion and downstream (Figure 10d, e and f) most of the laminar, the SA, and some of the SST simulations were able to accurately predict the $|\tau|$ over

most of the radius, but none of the turbulent flow models accurately captured the low wall shear stresses in the recirculation zone at the wall. This directly corresponds to errors in the velocity profiles in Figure 6e.

At Re_t = 3500, only the one laminar simulation was able to accurately model the shear stress in the inlet region corresponding to a parabolic velocity profile over the entire radius (Figure 11a). In general, most simulations agreed with experiment somewhat better in the collector and throat (Figure 11b and c) except near the wall, where the simulations varied considerably, particularly the KE models (but most of which were still within the experimental $CI_{95\%}$). In general, agreement was worse at the sudden expansion and downstream (Figure 11d, e, and f), with the laminar and SA model performing the best overall. At Re_t = 6500, the experimental shear stresses varied at the inlet due to slight differences in flow rate in this transitional regime (Re = 2167 at the inlet)[15] (Figure 12a). The simulations' shear stresses varied considerably at the collector and throat wall (Figure 12b and c), and considerable scatter was observed downstream (Figure 12d, e, and f). At this Re_t, no single model performed consistently well from inlet to outlet.

Wall Shear Stress

The distribution of wall shear stress ($\overline{WSS}$) is shown as a function of axial position in Figure 13. Even when omitting simulations with formatting or conservation law errors, the spread of results was large, especially downstream of the sudden expansion. Some of the 3D simulations also showed a band of values representing variations over the circumference of the nozzle. Errors in experimental data among the three labs was also observed, due to difficulties in imaging velocities close to the wall of the acrylic model. In general, the best agreement between the computations and experiments was in the nozzle throat. In contrast, most of the simulations

overestimated the $\overline{WSS}$ within the inlet representing parabolic laminar flow (Figure 13b, d, f, and h), due to assumptions of turbulence and/or non-parabolic inlet boundary conditions.

Downstream of the sudden expansion, the $\overline{WSS}$ was best matched by the laminar and KO simulations at Re_t = 500 (Figure 13a and b), with reattachment zones more consistent with previous data than the turbulent simulations.[8] At the transitional Re_t = 2000, (Figure 13c and d), the $\overline{WSS}$ in the recirculation zone within z = 0.05 m of the sudden expansion was also best approximated by the laminar simulation (which was transient in this case). The turbulent simulations overestimated the $\overline{WSS}$ in this region. At higher flow rates, Re_t = 3500 (Figure 13e and f), 5000 (not shown), and 6500 (Figure 13g and h), the measured recirculation zones were smaller, as expected.[8] The location of the reattachment points appeared to vary consistently with turbulence model (e.g., with the SST models closer to the sudden expansion than the KO models), but the maximum $\overline{WSS}$ within the recirculation zone was highly variable.

Grid Refinement Studies

The protocol for this interlaboratory study included a grid refinement study to be performed in the Sudden Expansion at Re_t = 5000. No specifications were given on the number of grid refinement levels to be used nor on the metric to be used in assessing which grid was to be used for the rest of the study. Only 16 of 28 participants provided grid refinement studies. For clarity, only six of the grid refinement studies provided are shown in Figure 14. Only some of the studies appeared to converge to a common solution. Furthermore, some of the studies did not converge monotonically (e.g., the one KO study). The converged solutions themselves varied and did not consistently approach the experimental data with increasing refinement, especially downstream of the sudden expansion. There was also no consistency on which grid density was used in the remainder of experiments, e.g. coarse, medium, or fine.

Validation Metrics

The global validation metric E_g, based on the axial velocity profiles is shown as a function of Re_t and grouped by families of turbulence models in Figure 15. Only simulations that met the conservation of mass criteria are included in this analysis (i.e., simulations with conservation of mass errors > 10% were omitted). The laminar simulations most accurately predicted the velocities at all Re_t. This surprising result can be explained by the local validation metric E_z as a function of z position shown in Figure 16: specifically, the laminar simulations did the best job of predicting velocities in the entrance region, nozzle throat, and just downstream of the sudden expansion, and failed primarily in the jet breakdown regions at $Re_t > 500$. Attempts were made to determine the statistical significance of E_g with respect to variables such as the inlet and outlet length, number of cells, experience levels, families of turbulence models, etc., but the independent variables were not significant in almost every case. Local errors reached a maximum just downstream of the sudden expansion due to the difficulties in accurately predicting velocities in the recirculation zones. In addition, low velocities tended to skew the error metric upward, due to the presence of velocity in the denominator of equation 2.

Discussion

The main goals of this study were to: 1) engage engineers and scientists in industry, academia, and government with interest in applying CFD to medical device development and regulation; 2) establish a set of experimentally validated benchmark computational models applicable to cardiovascular medical devices: and 3) use the models to develop standards and "best practices" for applying CFD to medical device regulatory activities. This paper presents results of the first such interlaboratory study in a benchmark developed for cardiovascular medical devices, consisting of flow in a nozzle model with a sudden expansion.

Among the 28 participants, there was a wide variety of CFD approaches and models employed, accompanied by an equally wide variation in results. Despite the use of turbulence models to help organize the Results section, *we do not endorse or recommend the use of any particular turbulence model over any other*. The data shown in Figure 16 clearly demonstrates that no single turbulence model is superior when applied to this problem. It is also important to note that successfully performing simulations on this benchmark nozzle model will not necessarily help in the regulatory review of either a similar or markedly different device. If CFD results are to be used to demonstrate a point about safety in a regulatory application, validation studies should be performed on the device under review. Note also that despite rumors to the contrary, *CFD studies are not currently required in device premarket notifications and applications submitted to the US FDA.*

Interestingly, a self-rated level of expertise by the project participants failed to correlate qualitatively with the validation metric; some self-rated "expert" CFD practitioners submitted results having large disagreement with experimental data, while self-rated "novice" users submitted results with above average agreement. We conclude that there was little uniformity of practice among the 28 participants.

In retrospect, we now understand that we requested too little detail from participants regarding their problem specification and solution techniques. We suspect that wide variations of wall treatments, boundary conditions, viscous mesh spacing, convergence criteria, time/space order of accuracies, etc. each contributed to the spread in the results. However, this information was either not collected, was not provided by all participants, or was not of a form to be analyzed. Future interlaboratory studies need to address some of these variability problems, and request more information on the methods used.

It is difficult to assign significance to a total dataset composed of only 28 entries. Moreover, the 28 entries are further segregated into specific groupings of smaller numbers, e.g., type of turbulence model or cell type. For example, the SA turbulence model had only one entry. If this particular user did well or poorly in applying the model, then the SA turbulence would be "graded" high or low, respectively, as compared to other turbulence models that may have had a wide spread of quality of application.

The sudden expansion nozzle proved to be an unexpectedly challenging test case, both for simulation and experiment. In fact, the Reynolds stresses had such wide variations that we elected not to attempt to correlate CFD results to the experimental data herein. As discussed in the Results section, radial velocity measurements and wall shear stresses were not reliably measured and were therefore omitted from this paper (but are available on our website). Challenges remain in avoiding or mitigating non-physical artifacts such as diffusive smearing of high frequency jet breakdown in the transitional regime due to the turbulence models used.

This study highlights the need for incompressible turbulence transition models or strategies. One fascinating finding was the excellent agreement of the single laminar model at transitional and turbulent Re_ts upstream of the turbulent jet breakdown. This was perhaps due to the fact that the lower four *inlet* Reynolds numbers were in the laminar regime (Table 1) and were so observed in the validation experiments.[15] While the exclusive use of a laminar model in these regimes is deemed inappropriate, its superior match with data in pre-transitional regions of the nozzle over fully turbulent solutions cannot be debated. The need for transitional models is further emphasized when one recognizes that many biomedical blood flow devices operate in the transitional regime. We noted that none of the participants submitted large eddy simulations (LES) for the transitional cases, perhaps due to a lack of personnel and computer resources

available to devote to this purely voluntary effort. As computing power continues to grow, adoption of LES techniques for complex biomedical problems will likely increase.

A substantial finding is that the CFD predicted shear stress distributions have wide variations among simulations, particularly the wall shear stress distributions. This has particular relevance and impact for blood damage modeling efforts. If shear stresses cannot be accurately predicted, efforts to develop a reliable and accurate numerical model of shear-induced blood damage are severely challenged or intractably hampered.

Finally, this study shows that CFD cannot be considered a "push-button" technology, not today nor likely in the near future. Furthermore, user experience and knowledge should play a critical role in the correct application of CFD, but evidently this is not always the case. In this study, some CFD "novices" submitted simulation datasets with better agreement than some CFD "experts." This points to several areas of research for the CFD community. Simple guidelines or best practices for biomedical CFD applications may yield improvements of simulation quality (however, this still needs to be demonstrated). Developers and companies have a prime opportunity to automate certain (to-be-determined) quality aspects of CFD analysis. It is imperative to undertake and openly publish high quality validation cases relevant to the biomedical community (for both fluid dynamics and blood damage) to help improve the quality of biomedical CFD simulations. This study is a step in this direction that we hope to continue, and is modeled after similar efforts in the aircraft,[37] ship,[38] and wind turbine[39] industries.

CFD can be a useful part of regulatory evaluation, both for premarket and postmarket studies. However, successful computational simulation of this nozzle model will not aid in a regulatory submission where the model is not applicable. The nozzle is a simple model, whereas CFD modeling of an actual device must take into consideration many complications: pulsatile

flow, transitional flows, secondary flows, sharp corners, the range of viscosity and hematocrit that the device is used, and the need for parameter sensitivity analysis of a simulation. An appropriate entrance and exit length must be chosen based on the in-use application; e.g., a ventricular assist device may have very short (and/or curved) entrance and exit conduits.

A brief summary of "Best Practices" identified in this study can be found in the Appendix.

Study Limitations

In defining the nozzle model and flow conditions, we tried to provide only the minimum information needed to properly set up the problem (for example, we specified the nozzle diameters, throat length, and cone geometry, but not the inlet and outlet lengths). We did not specify any guidance or recommendations for viscosity closure (turbulence) modeling. We also did not specify inlet boundary conditions. Some participants requested us to specify the inlet turbulence intensity, but we felt that would have influenced a choice in viscosity closure. Perhaps if we had specified the turbulence intensity, the variations in results may have been smaller. However, in our experiments, the inlet conditions were laminar at all throat Reynolds numbers except possibly 6500. Thus we would have had to specify zero turbulence intensity, which may have biased participants toward the use of laminar models.

In the original problem specifications, we inadvertently omitted asking participants to submit the inlet boundary conditions used. Later, we requested this information in an email update but by this time many participants had already submitted data. We eventually did receive boundary condition data from only about half the participants. Furthermore, some of the boundary condition data submitted were quite complicated.

We performed a preliminary comparison of the experimental and CFD-predicted

Reynolds stresses; however, the scatter was extremely large. The large variations seen may have been due to a number of factors, including a wide range of turbulence models, types of near wall turbulence treatment, levels of inlet turbulence intensity, and other boundary conditions. In addition, there were experimental variations in Reynolds stresses among the three labs. The low turbulence intensities seen (especially in the transitional regimes) also made comparisons problematic.

The experimental measurements of the radial velocity components suffered from noise where the radial velocities were low (e.g., the inlet tube). In the conical collector, the radial velocities were higher, and good measurements could be made. Downstream of the sudden expansion, however, PIV could not reliably measure the low radial velocities within the high velocity jet, because the time delays between images needed for low radial velocities allowed high speed particles in the axial jet to move out of the image. Thus we did not include the radial velocities in this report. However, they are available at our website, https://fdacfd.nci.nih.gov/.

This study posed many challenges. For the validation experiments, the main challenge was to minimize the laboratory-to-laboratory variability due to differences in the flow system configurations, measurement of the fluid properties, maintaining fluid property stability over the duration of the experiments, and reproducible fabrication of the acrylic model dimensions (which varied by less than 1%). The development of a standard operating protocol helped us minimize experimental variability, but could not completely eliminate it. In addition, the large size of the PIV images (> 10 GB for 1000 image pairs for all flow conditions) made sharing the raw PIV images between the labs impractical.

In the computational study, the blinding process made communication with individual participants difficult and time-consuming (especially with respect to correcting errors we could

not resolve ourselves). The volume of data made aggregation and analysis difficult, as resources prohibited expert database assistance. As noted above, there were areas we should have been more specific concerning the data requested. We struggled with methods for presenting data in a quantitative yet understandable way. Error metrics were of less use than we envisioned. Our sample size was small for the number of independent variables we collected (mesh size, turbulence model, etc.). However, we recognize how fortunate we are as a community that so many people were eager to volunteer valuable resources to this study, and we note that some participants may not have been able to devote as much time to the study as they would have liked.

Future Work

We will continue to analyze this data and present different aspects of it in the future. All data will be made available at https://fdacfd.nci.nih.gov/. Additional publications will cover the Conical Diffuser and blood damage aspects of this study. We plan to host further interlaboratory studies with models of interest to the biomedical community, e.g., a simplified rotary blood pump that has been developed and in which experiments have commenced.

Our group is contributing to relevant standards under active development (ASME V&V 40 - Verification and Validation in Computational Methods for Medical Devices, and AAMI MC84/Ed.1 -- Mechanical circulatory support device evaluation - Preclinical testing). We are also continuing to develop more detailed "best practices" on the use of CFD in regulatory efforts. These interlaboratory studies are essential in assessing the state of the art in biomedical computational fluid dynamics and will be helpful to the Food and Drug Administration and other regulatory bodies worldwide as well as to regulated industry, software developers, and academic partners.

Acknowledgements

We recognize and appreciate the support of the worldwide CFD community. In particular, the authors wish to thank our study participants: Yared Alemu, K. Amano, J. Ashton, Mehdi Behbahani, Catrin Bludszuweit-Philipp, Danny Bluestein, Parnian Boloori-Zadeh, Alistair Brown, Scott Corbett, Julien de Charentenay, D. de Zelicourt, Wade Dummer, K. Fraser, Leonid Goubergrits, Kurt Graichen, Linden Heflin, Darren Hitt, Marcus Hormes, Marc Horner, Xueying Huang, S. Krishnan, S. Kühne, Patricia Lawford, Ming Li, Z. Li, William Louisos, Takehisa Mori, Alex Medvedev, Joerg Mueller, Sei Murakami, Mariagrazia Pilotelli, M. Polster, N. Reuel, T. Schauer, E. Sirois, Ken Solen, Ulrich Steinseifer, Wei Sun, S. Takahashi, Masaaki Tamagawa, K. Tan, Dalin Tang, Ertan Taskin, Z. Teng, R. Toyao, Dan White, Z. Jon Wu, M. Xenos, and Ajit Yoganathan. We also thank Dr. Jason Schroeder of the Office of Surveillance and Bioinformatics, CDRH, FDA, for performing statistical analyses. This study was supported by the Food & Drug Administration's Critical Path Initiative. The mention of commercial products, their source, or their use in connection with material reported herein is not to be construed as either an actual or implied endorsement of such products by the U.S. Department of Health and Human Services.

Conflict of Interest Statement

None.

Appendix - Best Practices

CFD "Best Practices" identified in this study are listed below. These are not necessarily all-inclusive, nor do they guarantee an accurate simulation.

1. Identify the physics of the problem and choose the appropriate physical model.
2. Choose software carefully so that the physics of the problem can be properly captured.
3. If a turbulence model is used, justify the choice of the model and parameters used.
4. Correctly identify and quantify the necessary boundary conditions, initial conditions, material properties and other problem specifications.
5. Verify that the boundaries of the simulation do not interfere with the natural development and physical character of the flow.
6. Confirm that the simulation has numerically converged via residual reductions and/or monitoring of some physically relevant fluid flow quantity at a relevant probe point (or points) and/or surface location(s). For example, residuals of the algebraic solver for each dependent variable should be plotted. For steady simulations, three orders of magnitude drop is typically sufficient for an engineering analysis. Corresponding iterative convergence of both point and integral metrics should be plotted to determine the iterative error. For unsteady simulations, iterative convergence of algebraic solvers must be assessed, as well as the impact of outer correctors, and non-orthogonal correctors on the time-accuracy.
7. Perform a proper grid refinement study, preferably by doubling and quadrupling the grid density over the production grid. Choose reasonable variables of interest for convergence monitoring and a logical rationale for choosing the "best" mesh. In general, grid refinement studies are beneficial, but insufficient to ensure good results.

8. Validate the simulation with trustworthy experimental measurements of both local and global variables, using quantitative measures rather than side-by-side comparisons of contour plots. A global performance metric (e.g., pressure drop across a device) is rarely by itself a useful validation metric.
9. Validation should be performed against like or similar types of models.
10. Anisotropic boundary layer meshing used to resolve viscous effects should have mesh spacing that can be justified via physical reasoning.
11. Mesh cell type (e.g., triangular, tetrahedral, hexahedral) should be chosen with knowledge that different cell types have different numerical characteristics (e.g., artificial dissipation, limited order of spatial accuracies, etc.)
12. Portions of the flow domain meshed with a higher density than other regions should be chosen carefully with guidance from the intermediate solutions.
13. Make sure the results are reasonable and/or intuitive from a fluid mechanics point of view.
14. Ensure that basic conservation laws are obeyed. For example, in this study, the conservation of mass was checked by integrating velocity profiles. Other methods may need to be developed in other problems.
15. If available, use existing theoretical solutions (e.g., steady and unsteady pipe flow) and benchmark validation data (e.g., backward facing step) to check accuracy, simulation protocol, selection of parameters, etc. For example, the present sudden expansion case produces similar results to those found previously.[8]
16. When reporting results, provide plots with legends and labels. Contour plots may not be the best format for showing experimental validation or mesh convergence;

quantitative results should be provided.

17. Some of the elementary errors made in this study suggest that training and experience are essential components to performing accurate simulations.

List of Tables

List of Figures

-0.048 m, c) z = -0.008 m, d) z = 0.008 m, e) z = 0.024 m, and f) z = 0.080 m. Lines are CFD results plotted against turbulence model used (simulations with conservation of mass errors > 10% are omitted). Symbols are interpolated experimental means ± 95% confidence interval.

Figure 6. Axial velocity profiles for throat Reynolds number = 2000: a) z = -0.088 m, b) z = -0.008 m, c) z = 0.008 m, d) z = 0.032 m, e) z = 0.060 m, and f) z = 0.080 m. Lines are CFD results plotted against turbulence model used (simulations with conservation of mass errors > 10% are omitted). Symbols are interpolated experimental means ± 95% confidence interval.

Figure 7. Axial velocity profiles for throat Reynolds number = 3500: a) z = -0.088 m, b) z = -0.048 m, c) z = -0.008 m, d) z = 0.008 m, e) z = 0.024 m, and f) z = 0.080 m. Lines are CFD results plotted against turbulence model used (simulations with conservation of mass errors > 10% are omitted). Symbols are interpolated experimental means ± 95% confidence interval.

Figure 8. Axial velocity profiles for throat Reynolds number = 6500: a) z = -0.088 m, b) z = -0.048 m, c) z = -0.008 m, d) z = 0.008 m, e) z = 0.024 m, and f) z = 0.080 m. Lines are CFD results plotted against turbulence model used (simulations with conservation of mass errors > 10% are omitted). Symbols are interpolated experimental means ± 95% confidence interval.

Figure 9. Shear-stress magnitude profiles for throat Reynolds number = 500: a) z = -0.088 m, b) z = -0.048 m, c) z = -0.008 m, d) z = 0.0 m, e) z = 0.008 m, and f) z = 0.024 m. Lines are CFD results plotted against turbulence model used (simulations with conservation of mass errors > 10% are omitted). Symbols are interpolated experimental means ± 95% confidence interval.

Figure 10. Shear-stress magnitude profiles for throat Reynolds number = 2000: a) z = -0.088 m, b) z = -0.048 m, c) z = -0.008 m, d) z = 0.0 m, e) z = 0.008 m, and f) z = 0.024 m. Lines are CFD results plotted against turbulence model used (simulations with conservation of mass errors > 10% are omitted). Symbols are interpolated experimental means ± 95% confidence interval.

Figure 11. Shear-stress magnitude profiles for throat Reynolds number = 3500: a) z = -0.088 m, b) z = -0.048 m, c) z = -0.008 m, d) z = 0.0 m, e) z = 0.008 m, and f) z = 0.024 m. Lines are CFD results plotted against turbulence model used (simulations with conservation of mass errors > 10% are omitted). Symbols are interpolated experimental means ± 95% confidence interval.

Figure 12. Shear-stress magnitude profiles for throat Reynolds number = 6500: a) z = -0.088 m, b) z = -0.048 m, c) z = -0.008 m, d) z = 0.0 m, e) z = 0.008 m, and f) z = 0.024 m. Lines are CFD results plotted against turbulence model used (simulations with conservation of mass errors > 10% are omitted). Symbols are interpolated experimental means ± 95% confidence interval.

Figure 13. Wall-shear stress (WSS) for throat Reynolds number = 500 (a, b); 2000 (c, d); 3500 (e, f); and 6500 (g, h). Panels in the right column are magnified versions of those in the left column, showing the WSS near the sudden expansion. Colored dots are CFD results plotted against turbulence model used (simulations with conservation of mass errors > 10% are omitted, as are simulations with obvious formatting errors that could not be corrected). Symbols are experimental means ± 95% confidence interval (n = 9 - 12).

Figure 14. Selected grid refinement studies (with conservation of mass errors less than 10%) performed at throat Reynolds number = 5000, showing axial velocity along nozzle centerline downstream of sudden expansion. Each color is a separate participant's study. The production grid used is outlined by a box in the legend. Symbols are corresponding experiments (3 repeated experiments from one lab, and 1 from each of two additional labs).

Figure 15. Global validation metric E_g (averaged by turbulence model) as a function of throat Reynolds number. Sample size is variable (see Table 3). Simulations with conservation of mass errors > 10% are omitted.

Figure 16. Local validation metric E_z (averaged by turbulence model) as a function of throat

Reynolds number (Re_t) and z position of cross-sectional cut: a) $Re_t = 500$; b) $Re_t = 2000$; c) $Re_t = 3500$; d) $Re_t = 5000$; e) $Re_t = 6500$. Sample size is variable (see Table 3). Simulations with conservation of mass errors > 10% are omitted.

References

1. Bludszuweit C. Model for a general mechanical blood damage prediction. Artif Organs. 1995;19:583-9.
2. Burgreen GW, Antaki JF, Wu ZJ, Holmes AJ. Computational fluid dynamics as a development tool for rotary blood pumps. Artif Organs. 2001;25;336-40.
3. De Wachter D, Verdonck P. Numerical calculation of hemolysis levels in peripheral hemodialysis cannulas. Artif Organs. 2002;26:576-82.
4. Dumont K, Vierendeels J, Kaminsky R, van Nooten G, Verdonck P, Bluestein D. Comparison of the hemodynamic and thrombogenic performance of two bileaflet mechanical heart valves using a CFD/FSI model. J Biomech Eng. 2007;129:558-65.
5. Dwyer HA, Matthews PB, Azadani A, Jaussaud N, Ge L, Guy TS, Tseng EE. Computational fluid dynamics simulation of transcatheter aortic valve degeneration. Interact Cardiovasc Thorac Surg. 2009;9:301-8.
6. Fallon AM, Dasi LP, Marzec UM, Hanson SR, Yoganathan AP. Procoagulant properties of flow fields in stenotic and expansive orifices. Ann Biomed Engr. 2008;36:1-13.
7. Fiore GB, Morbiducci U, Ponzini R, Redaelli A. Bubble tracking through computational fluid dynamics in arterial line filters for cardiopulmonary bypass. ASAIO J. 2009;55:438-44.
8. Gach HM, Lowe IJ. Measuring flow reattachment lengths downstream of a stenosis using MRI. J Magn Reson Imaging. 2000;12:939-48.
9. Garon A, Farinas MI. Fast three-dimensional numerical hemolysis approximation. Artif Organs. 2004;28:1016-25.
10. Ge L, Leo HL, Sotiropoulos F, Yoganathan AP. Flow in a mechanical bileaflet heart

valve at laminar and near-peak systole flow rates: CFD simulations and experiments. J Biomech Eng. 2005;127:782-97

11. Giersiepen M, Wurzinger LJ, Opitz R, Reul H. Estimation of shear stress-related blood damage in heart valve prostheses - in vitro comparison of 25 aortic valves. Intl J Artif Organs. 1990;13:300-6.

12. Goubergrits L, Affeld K. Numerical estimation of blood damage in artificial organs. Artif Organs. 2004;28:499-507.

13. Grigioni M, Morbiducci U, D'Avenio G, Benedetto GD, Gaudio CD. A novel formulation for blood trauma prediction by a modified power-law mathematical model. Biomech Model Mechanobiol. 2005;4:249-60.

14. Gross JM, Shu MC, Dai FF, Ellis J, Yoganathan AP. A microstructural flow analysis within a bileaflet mechanical heart valve hinge. J Heart Valve Dis. 1996;5:581-90.

15. Hariharan P, Giarra M, Reddy V, Day S, Manning KB, Deutsch S, Stewart SFC, Myers MR, Berman MR, Burgreen GW, Paterson EG, Malinauskas RA. Experimental particle image velocimetry protocol and results database for validating computational fluid dynamic simulations of the FDA benchmark nozzle model. J Biomech Eng. 2011;133:041002.

16. He Y, Duraiswamy N, Frank AO, Moore JE Jr. Blood flow in stented arteries: a parametric comparison of strut design patterns in three dimensions. J Biomech Eng. 2005;127:637-47.

17. Hinds MT, Park YJ, Jones SA, Giddens DP, Alevriadou BR. Local hemodynamics affect monocytic cell adhesion to a three-dimensional flow model coated with E-selectin. J Biomech. 2001;34:95-103.

18. Izraelev V, Weiss WJ, Fritz B, Newswanger RK, Paterson EG, Snyder A, Medvitz RB, Cysyk J, Pae WE, Hicks D, Lukic B, Rosenberg G. A passively suspended Tesla pump left ventricular assist device. ASAIO J 2009;55:556-61.

19. Kameneva MV, Burgreen GW, Kono K, Repko B, Antaki JF, Umezu M. Effects of turbulent stresses upon mechanical hemolysis: experimental and computational analysis. ASAIO J. 2004;50:418-23.

20. Longest PW, Kleinstreuer C. Comparison of blood particle deposition models for non-parallel flow domains. J Biomech. 2003;36:421-30.

21. Nobili M, Morbiducci U, Ponzini R, Del Gaudio C, Balducci A, Grigioni M, Maria Montevecchi F, Redaelli A. Numerical simulation of the dynamics of a bileaflet prosthetic heart valve using a fluid-structure interaction approach. J Biomech. 2008;41:2539-50.

22. Oberkampf WL, Barone MF. Measures of agreement between computation and experiment: validation metrics. J Comput Phys. 2006;217:5-36.

23. Oberkampf WL, Trucano TG, Hirsch C. Verification validation and predictive capability in computational engineering and physics. Appl Mech Rev. 2004;57:345-84.

24. Pant S, Bressloff NW, Forrester AI, Curzen N. The influence of strut-connectors in stented vessels: a comparison of pulsatile flow through five coronary stents. Ann Biomed Eng. 2010;38:1893-907.

25. Pinotti M, Rosa ES. Computational prediction of hemolysis in a centrifugal ventricular assist device. Artif Organs. 1995;19:267-73.

26. Raz S, Einav S, Alemu Y, Bluestein D. DPIV prediction of flow induced platelet activation-comparison to numerical predictions. Ann Biomed Eng. 2007;35:493-504.

27. Sutera SP. Flow-induced trauma to blood cells. Circulation Res. 1977:41:2-11.

28. Takano T, Schulte-Eistrup S, Kawahito S, Maeda T, Nonaka K, Linneweber J, Glueck J, Fujisawa A, Makinouchi K, Yokokawa M, Nosé Y. Inlet port positioning for a miniaturized centrifugal blood pump. Artif Organs. 2002;26:45-8.

29. Tamagawa M, Kaneda H, Hiramoto M, Nagahama S. Simulation of thrombus formation in shear flows using lattice boltzmann method. Artif Organs. 2009;33:604-10.

30. Williams AR. Shear-induced fragmentation of human erythrocytes. Biorheology. 1973;10:303-11.

31. Wu J, Antaki JF, Wagner WR, Snyder TA, Paden BE, Borovetz HS. Elimination of adverse leakage flow in a miniature pediatric centrifugal blood pump by computational fluid dynamics-based design optimization. ASAIO J. 2005;51:636-43.

32. Wu J, Paden BE, Borovetz HS, Antaki JF. Computational fluid dynamics analysis of blade tip clearances on hemodynamic performance and blood damage in a centrifugal ventricular assist device. Artif Organs. 2010;34:402-11.

33. Xenos M, Girdhar G, Alemu Y, Jesty J, Slepian M, Einav S, Bluestein D. Device Thrombogenicity Emulator (DTE) – Design optimization methodology for cardiovascular devices: A study in two bileaflet MHV designs. J Biomech. 2010;43:2400-9.

34. Xu Z, Chen N, Kamocka MM, Rosen ED, Alber M. A multiscale model of thrombus development. J R Soc Interface. 2008;5:705-22.

35. Yano T, Sekine K, Mitoh A, Mitamura Y, Okamoto E, Kim DW, Nishimura I, Murabayashi S, Yozu R. An estimation method of hemolysis within an axial flow blood pump by computational fluid dynamics analysis. Artif Organs. 2003;27:920-5.

36. Yeleswarapu KK, Antaki JF, Kameneva MV, Rajagopal KR. A mathematical model for

shear-induced hemolysis. Artif Organs. 1995;19:576-582.

37. http://aaac.larc.nasa.gov/tsab/cfdlarc/aiaa-dpw/

38. http://www.iihr.uiowa.edu/gothenburg2000/index.html

39. http://wind.nrel.gov/amestest/

Table 1. Flow rates and Reynolds numbers used in simulations.

Flow Rate (m^3/s)	Throat Reynolds Number (Re_t)	Inlet Reynolds Number (Re_i)
$5.21x10^6$	500	167
$2.08x10^5$	2000	667
$3.64x10^5$	3500	1167
$5.21x10^5$	5000	1667
$6.77x10^5$	6500	2167

Table 2. Distribution of families of turbulence models used vs. laminar simulations.

Re_t	k-omega/SST	Spalart-Allmaras	laminar	k-omega	k-epsilon
500	6	0	13	2	7
2000	10	1	7	2	8
3500	12	1	2	2	11
5000	12	1	2	2	11
6500	12	1	2	3	10

Table 3. Global Error Metric (E_g) vs. Re_t and Turbulence Model Shown in Figure 15. Simulations with conservation of mass errors > 10% are omitted.

Turbulence Model:	Throat Reynold Number (Re_t)									
	500		2000		3500		5000		6500	
	Eg Mean (S.D.)	n	Eg Mean (S.D.)	n	Eg Mean (S.D.)	n	Eg Mean (S.D.)	n	Eg Mean (S.D.)	n
k-epsilon	1.58 (0.18)	3	2.30 (0.37)	5	3.23 (0.33)	3	2.29 (0.39)	3	2.11 (0.75)	4
k-omega	0.31 (0.00)	1	1.38 (0.00)	1	1.73 (0.00)	1	0.95 (0.00)	1	1.12 (0.05)	2
laminar	0.34 (0.30)	7	0.55 (0.06)	3	0.74 (0.00)	1	0.89 (0.00)	1	0.83 (0.00)	1
Spalart Allmaras	-	-	1.22 (0.00)	1	1.55 (0.00)	1	1.20 (0.00)	1	1.52 (0.00)	1
SST	0.59 (0.38)	6	1.68 (0.63)	9	2.36 (0.73)	9	1.57 (0.35)	10	1.92 (0.63)	10

colour figure
Click here to download high resolution image

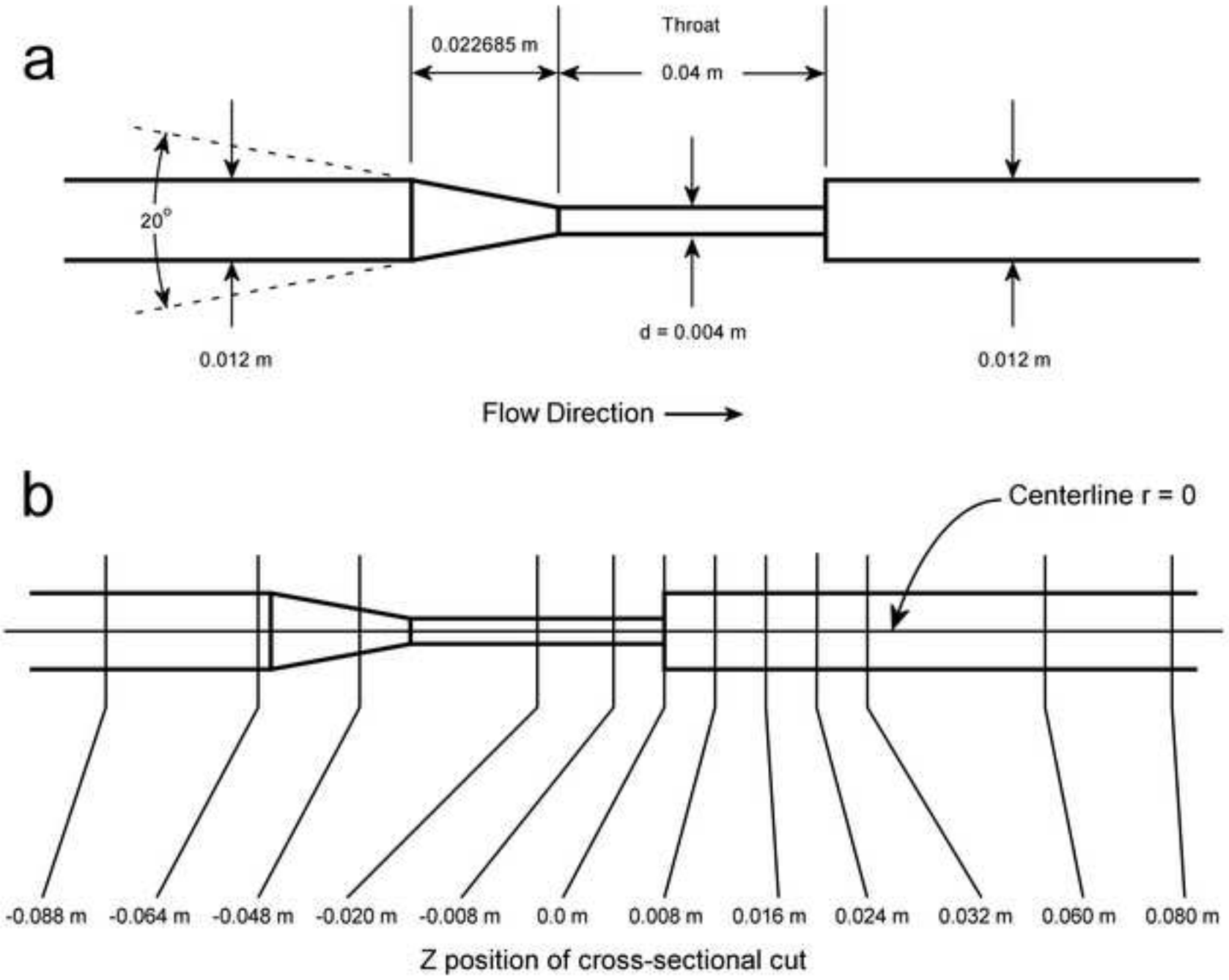

colour figure
Click here to download high resolution image

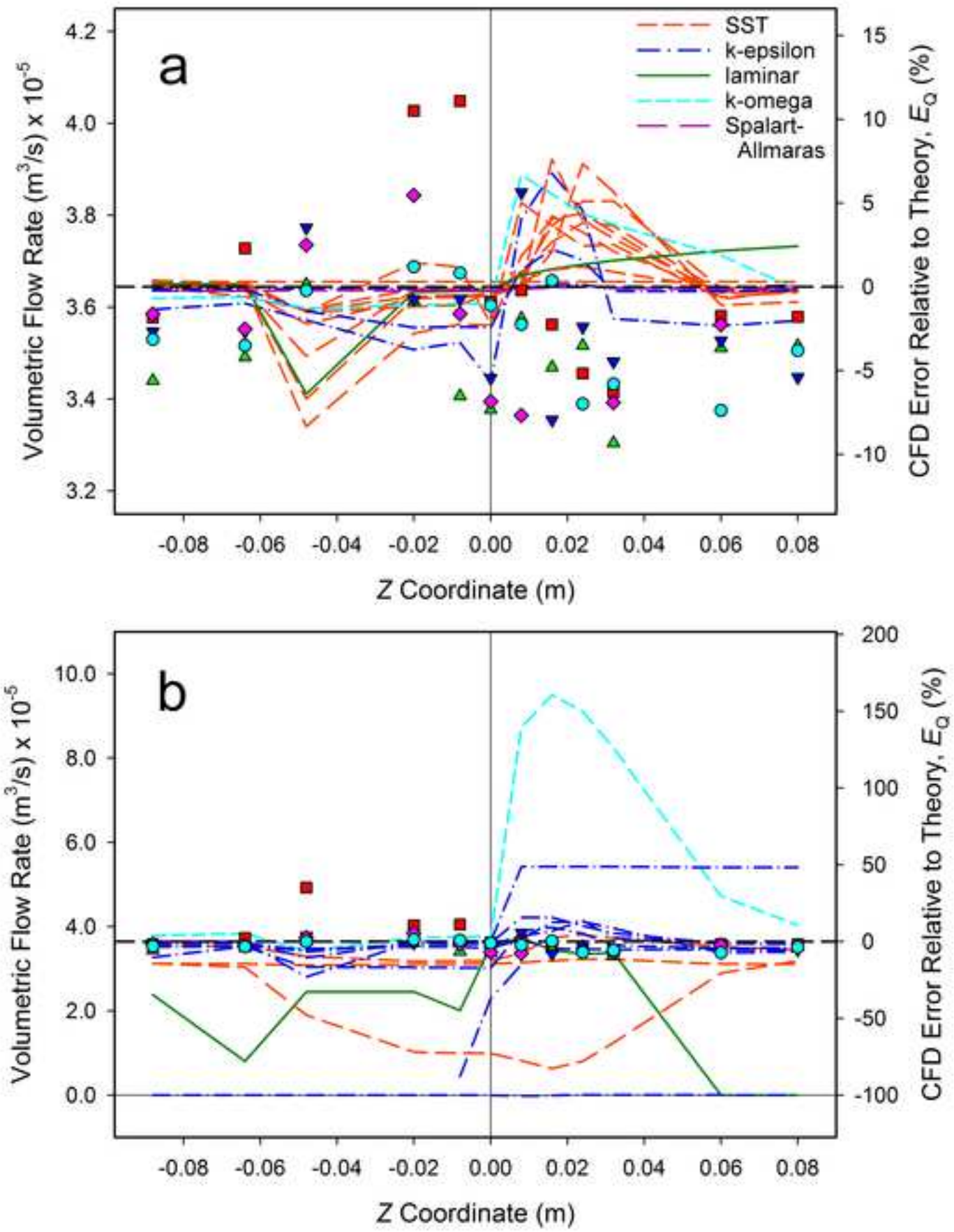

colour figure
Click here to download high resolution image

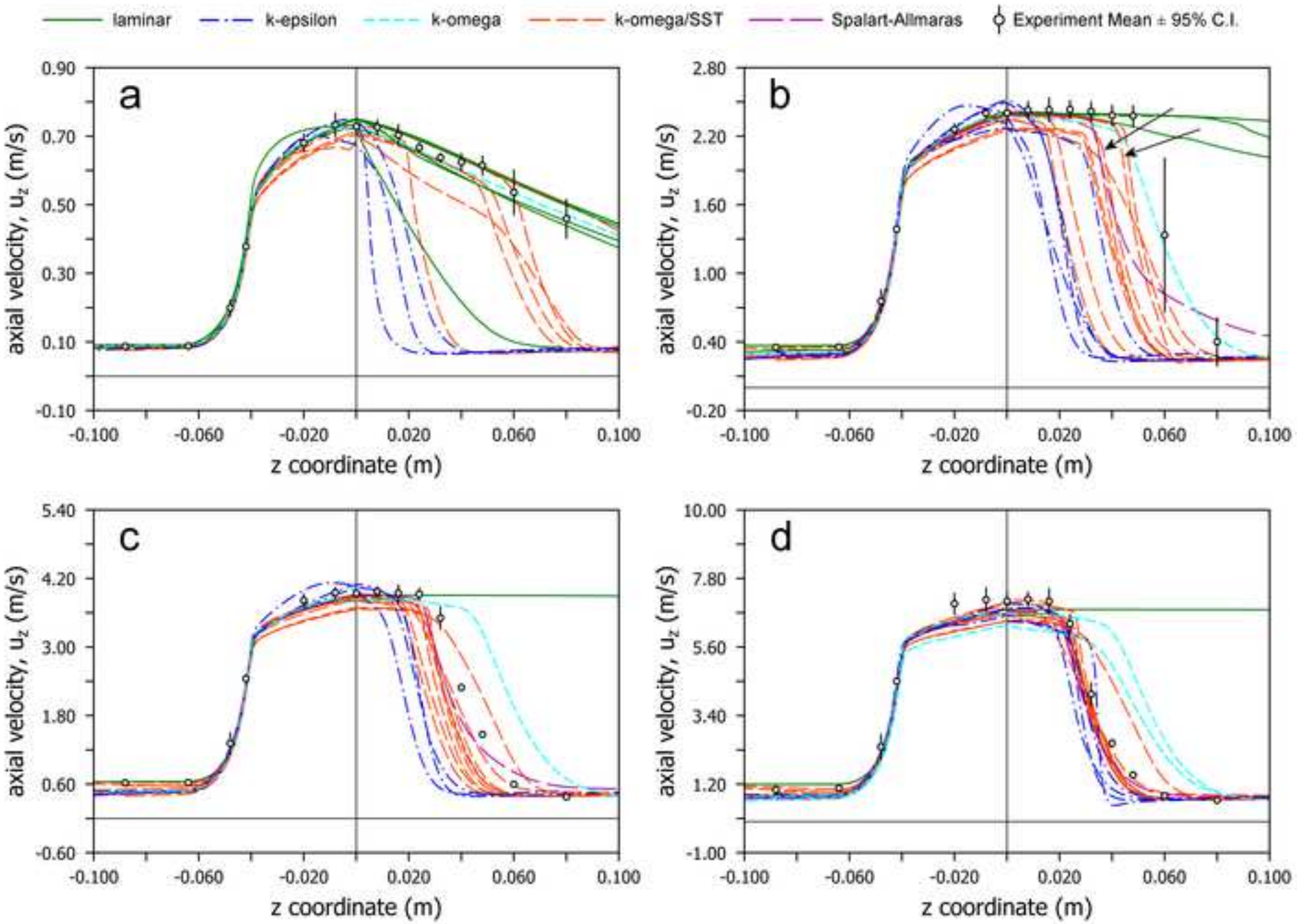

colour figure
Click here to download high resolution image

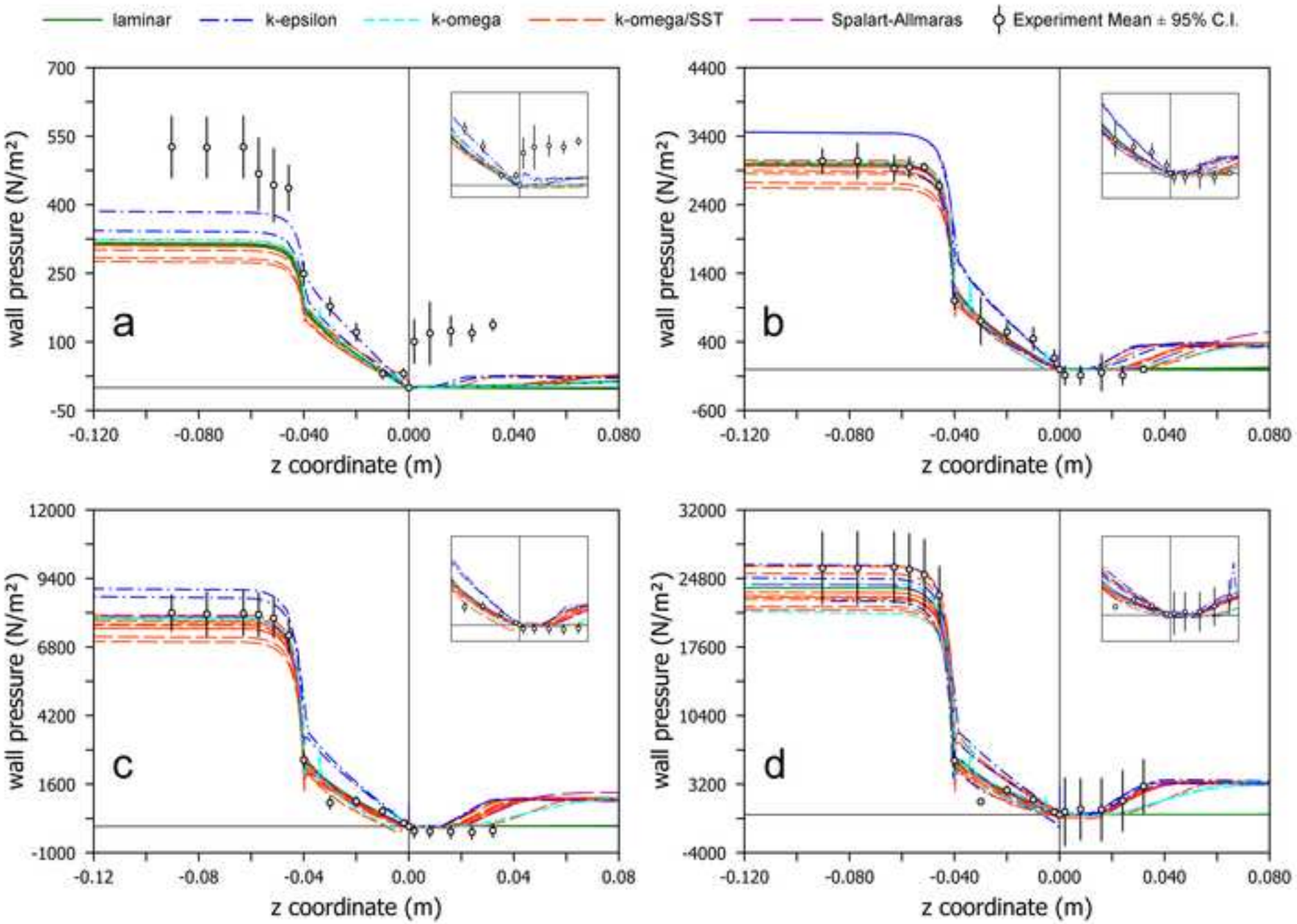

colour figure
Click here to download high resolution image

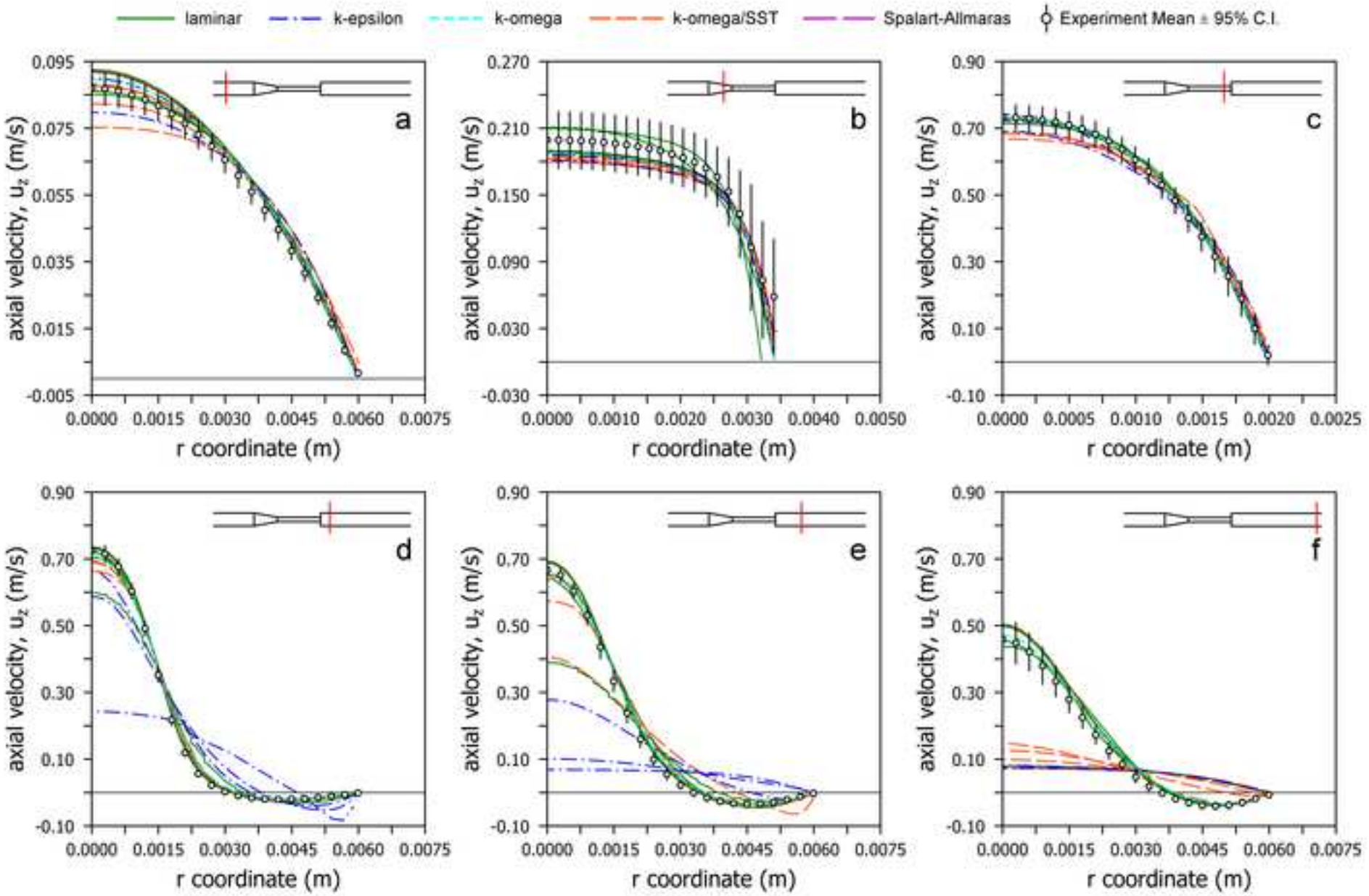

colour figure
Click here to download high resolution image

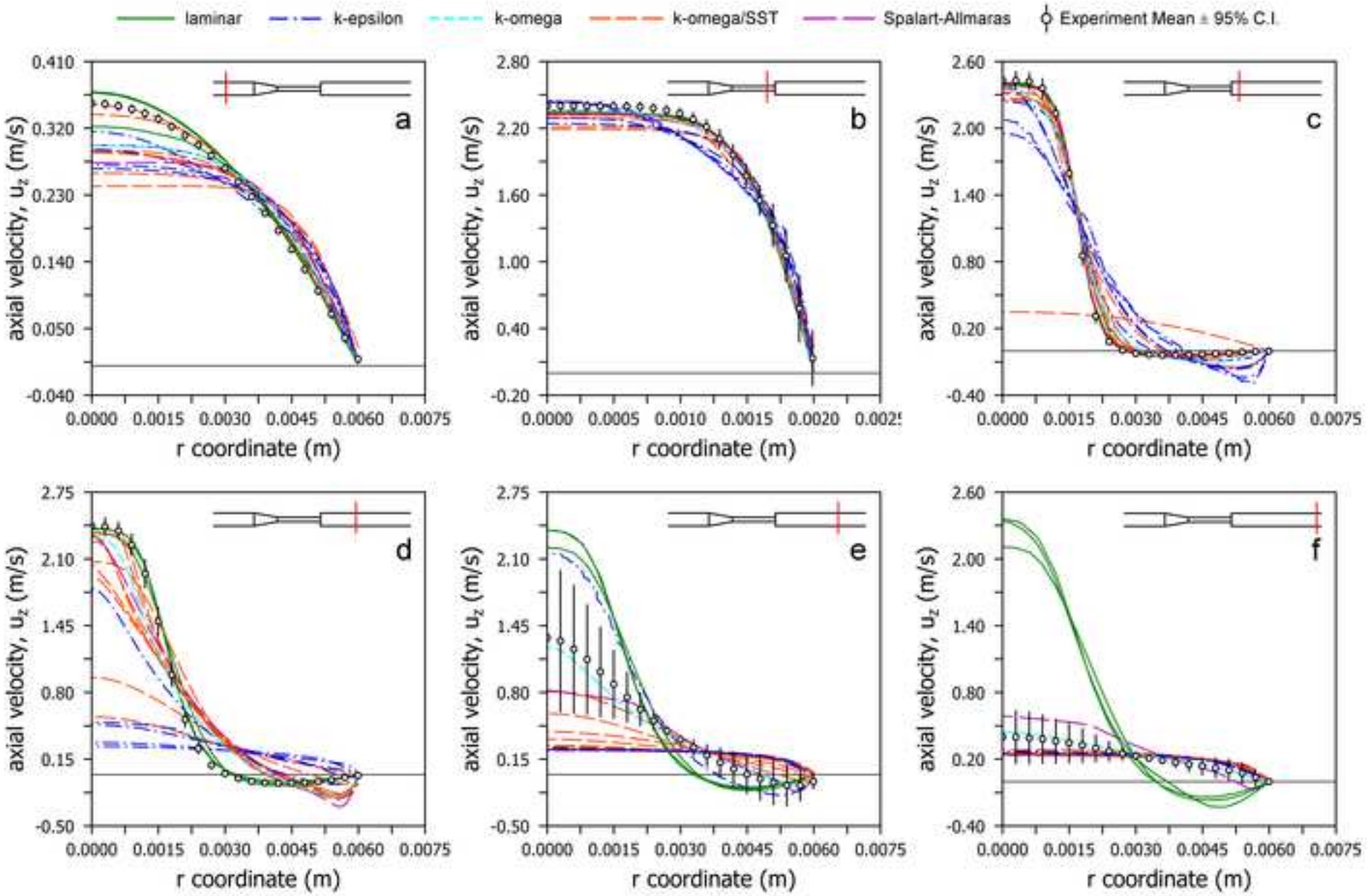

colour figure
Click here to download high resolution image

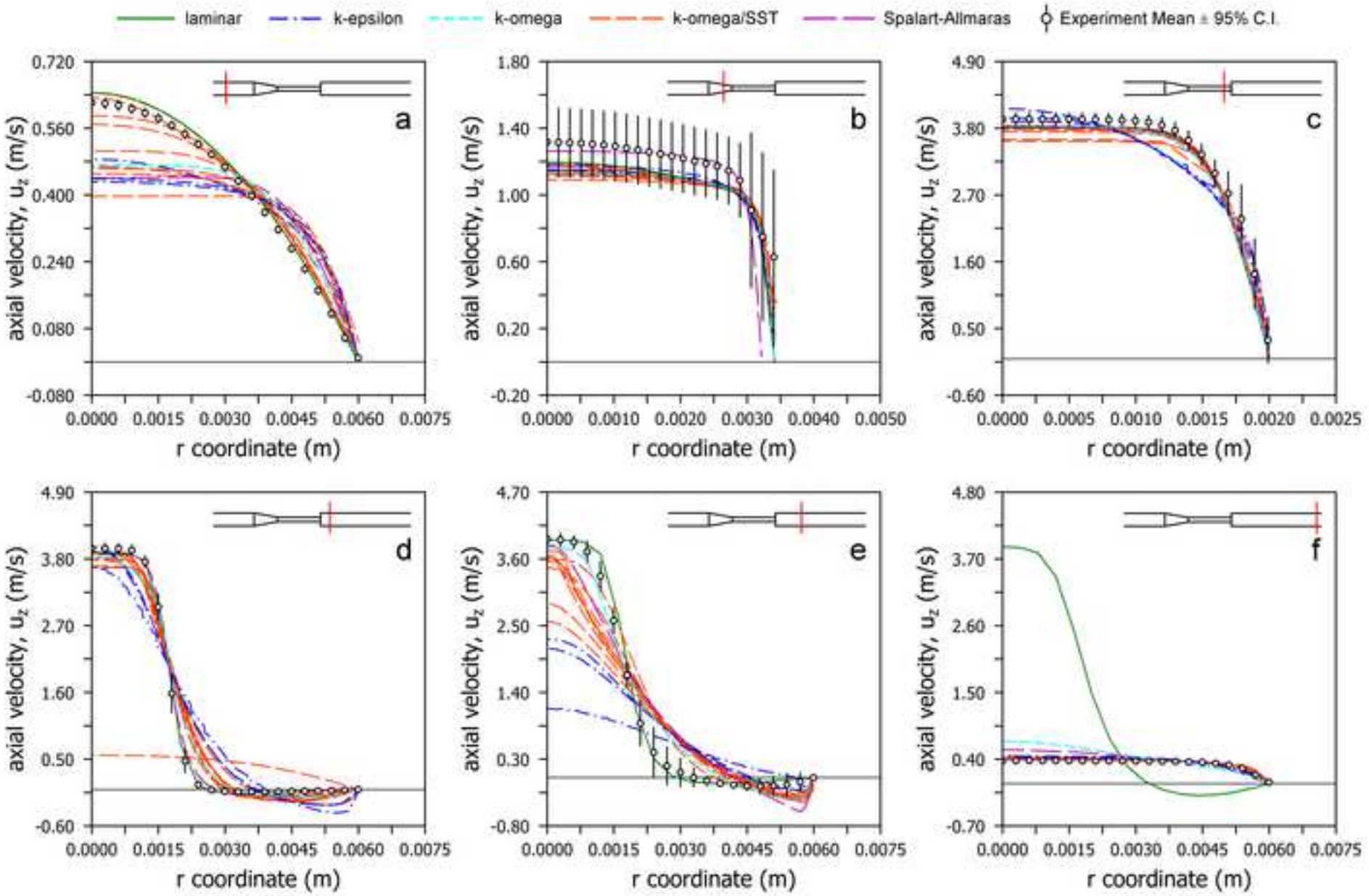

colour figure
Click here to download high resolution image

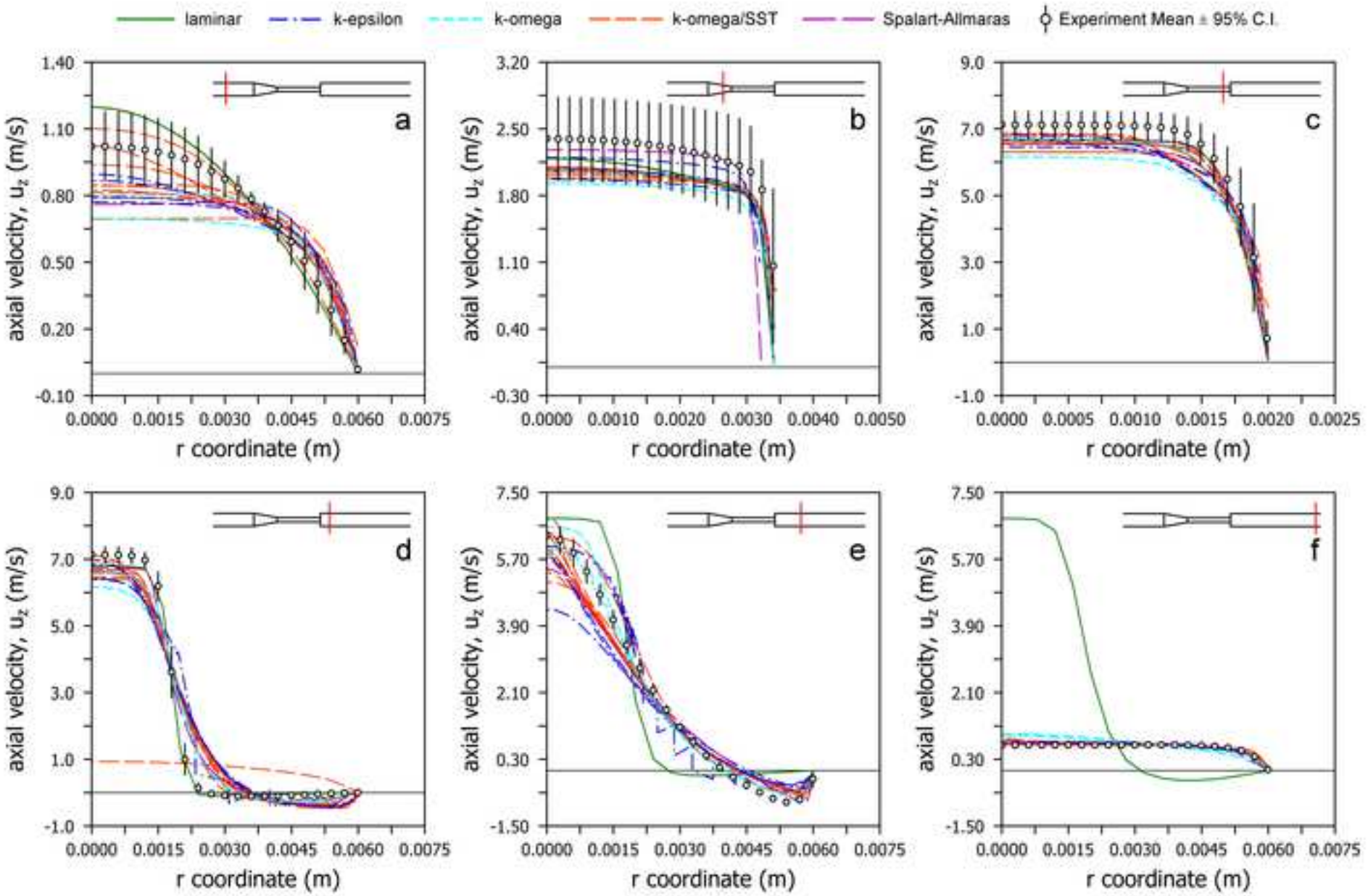

colour figure
Click here to download high resolution image

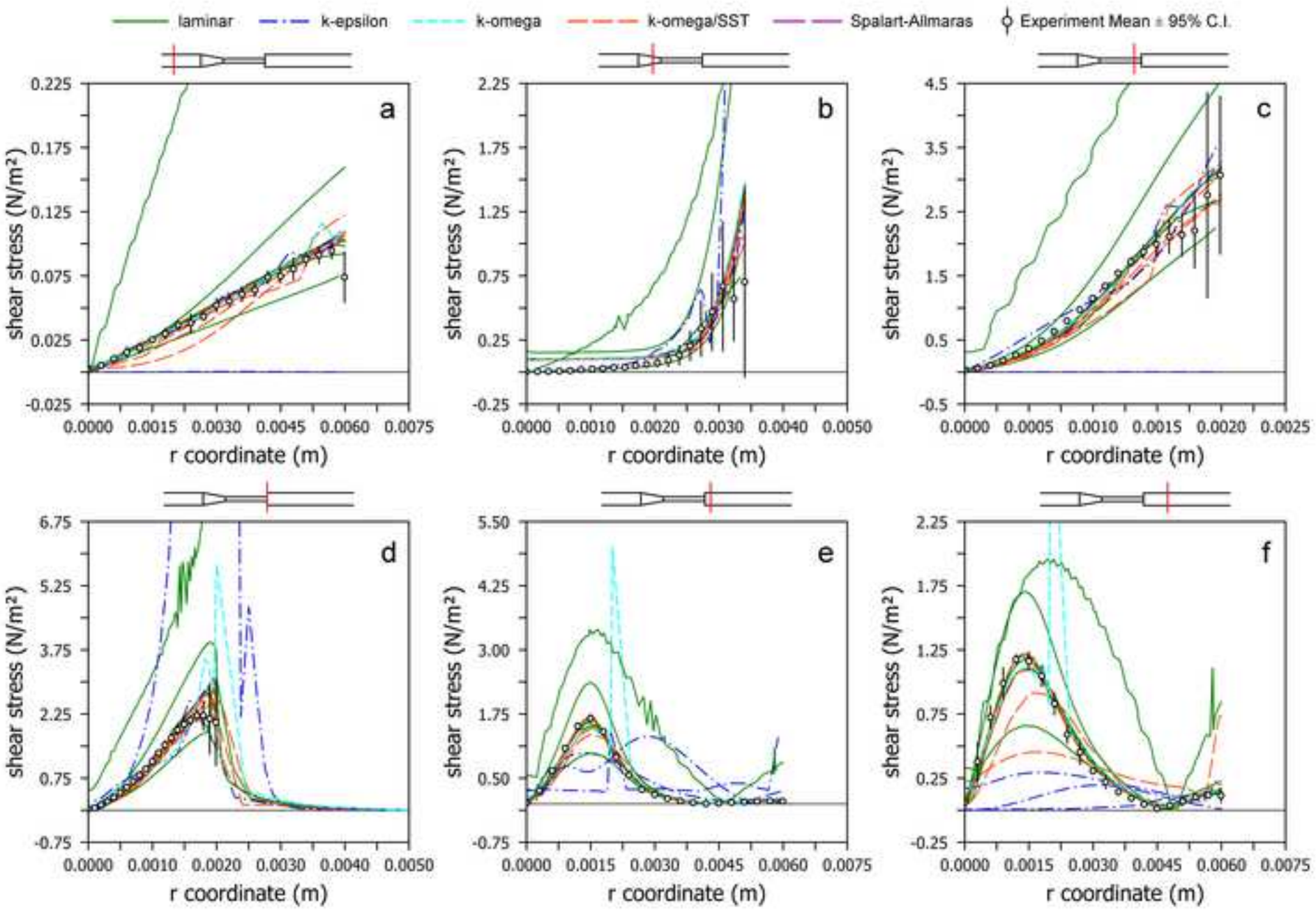

colour figure
Click here to download high resolution image

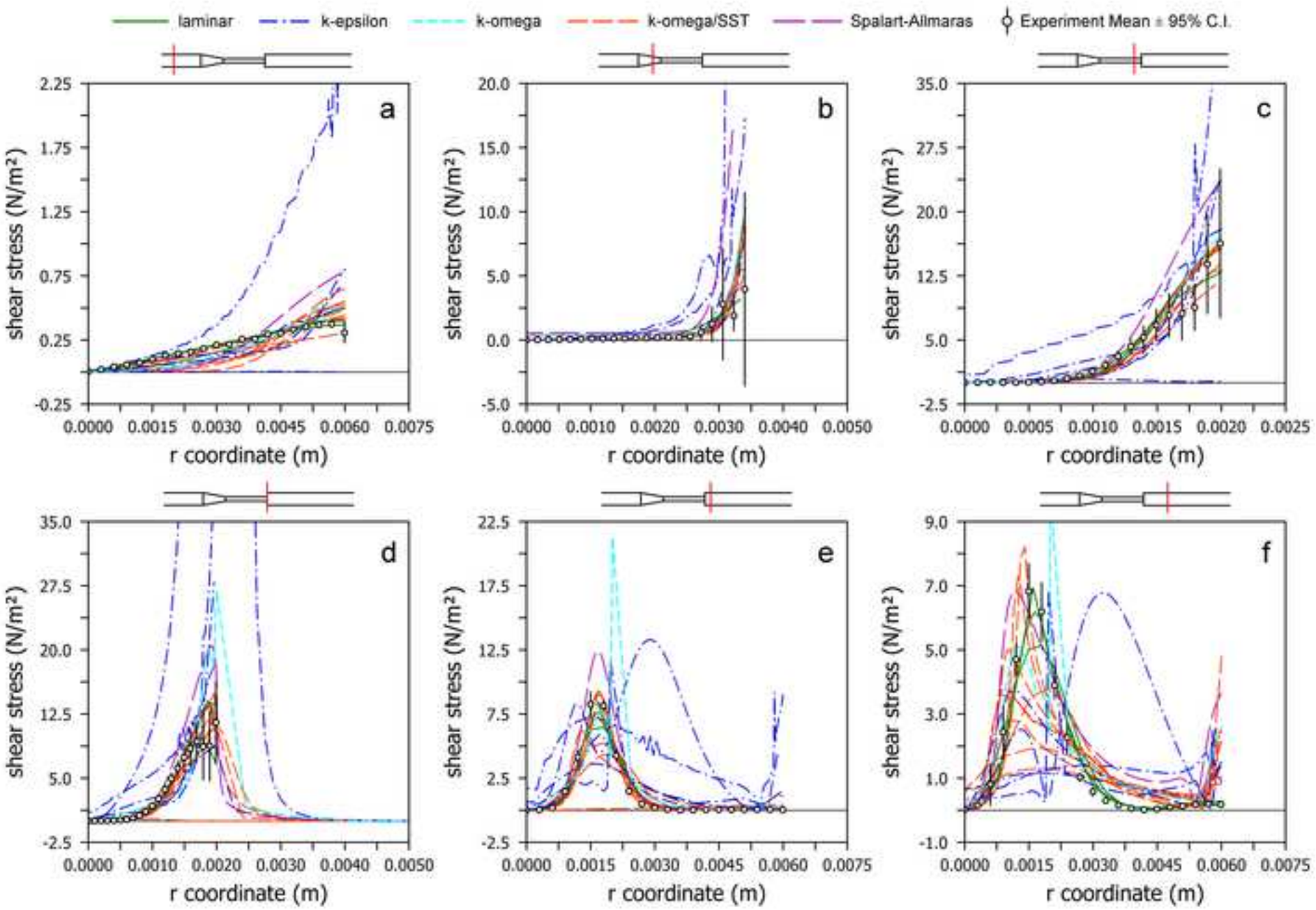

colour figure
Click here to download high resolution image

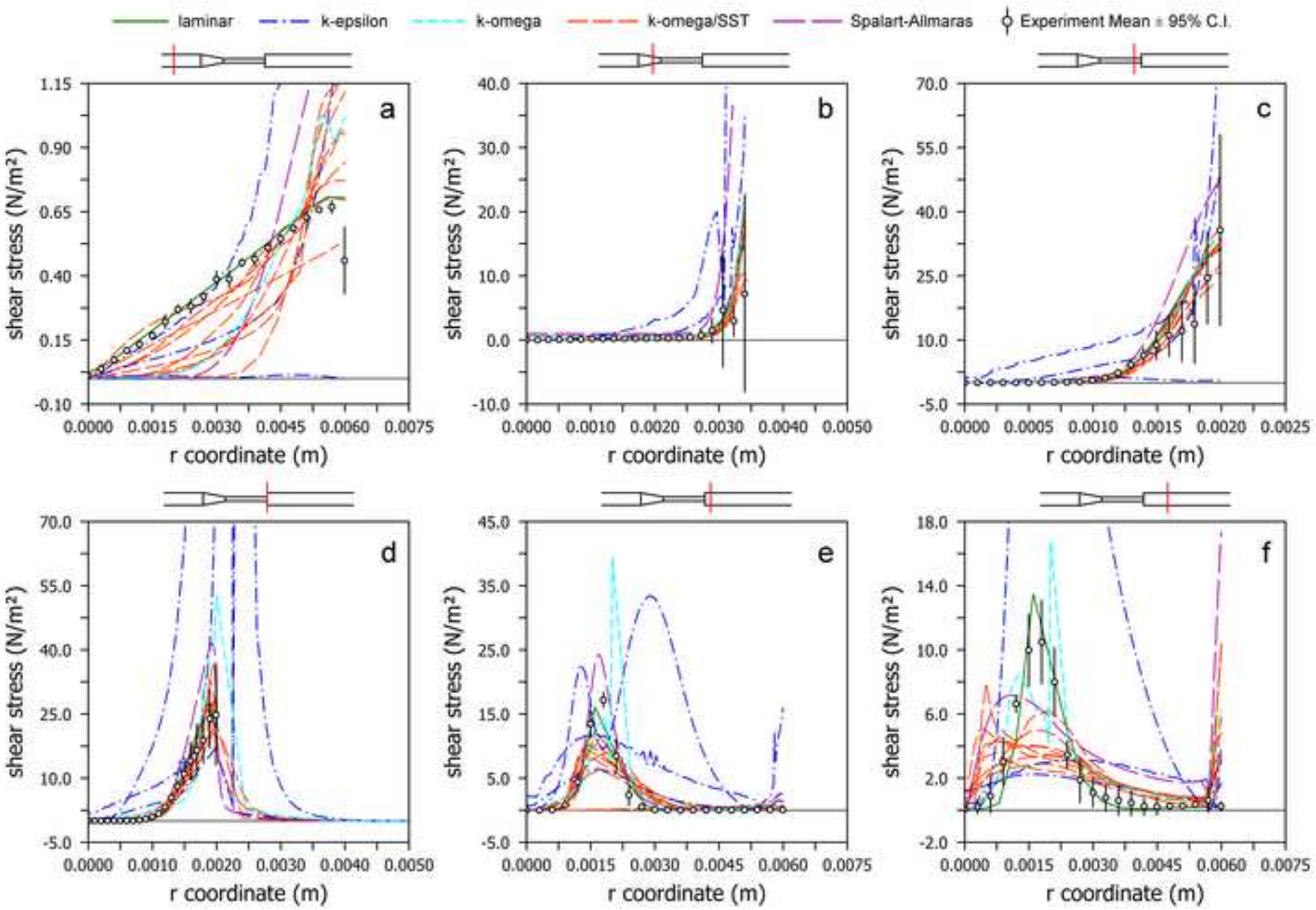

colour figure
Click here to download high resolution image

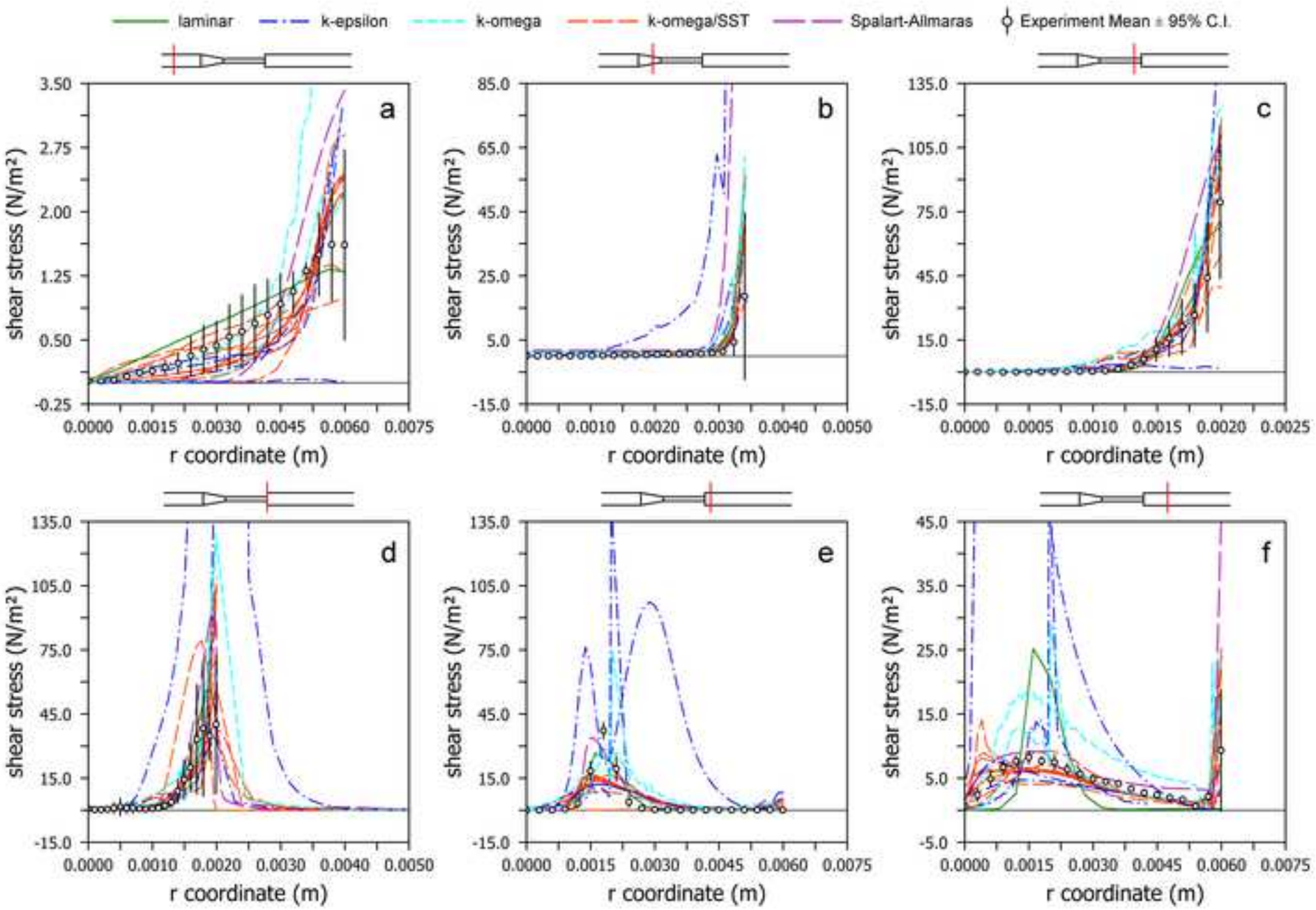

colour figure

Click here to download high resolution image

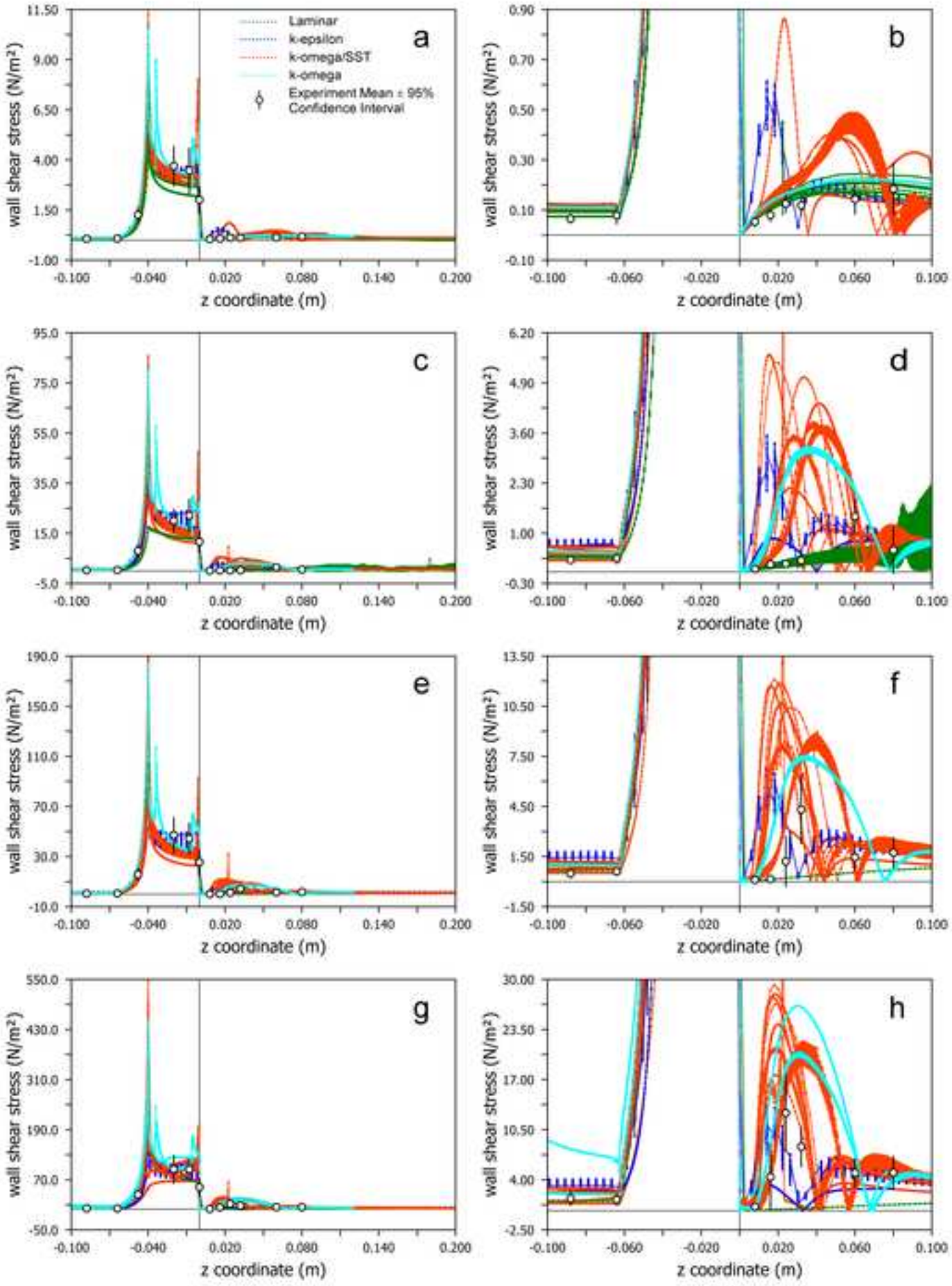

colour figure
Click here to download high resolution image

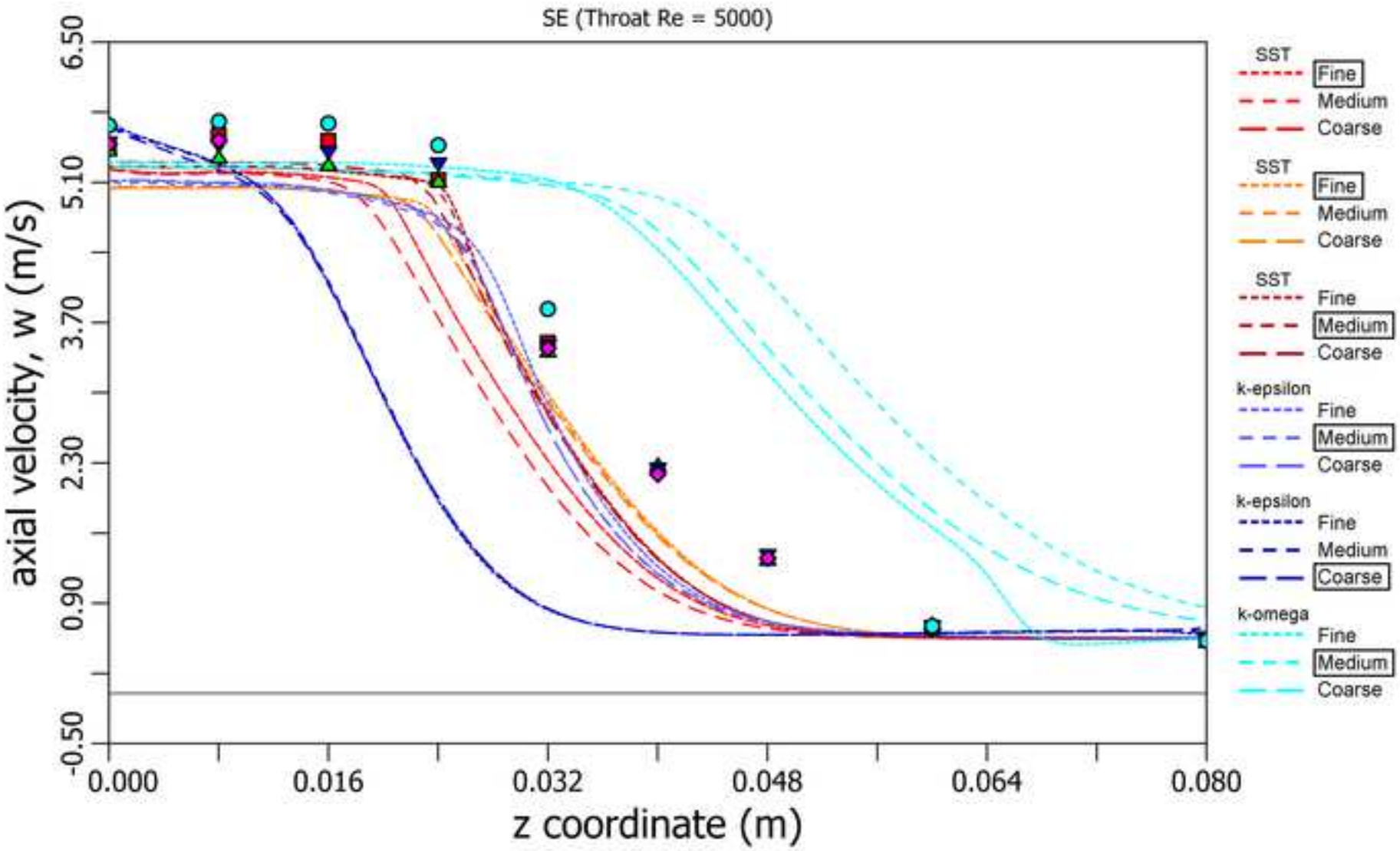

colour figure
Click here to download high resolution image

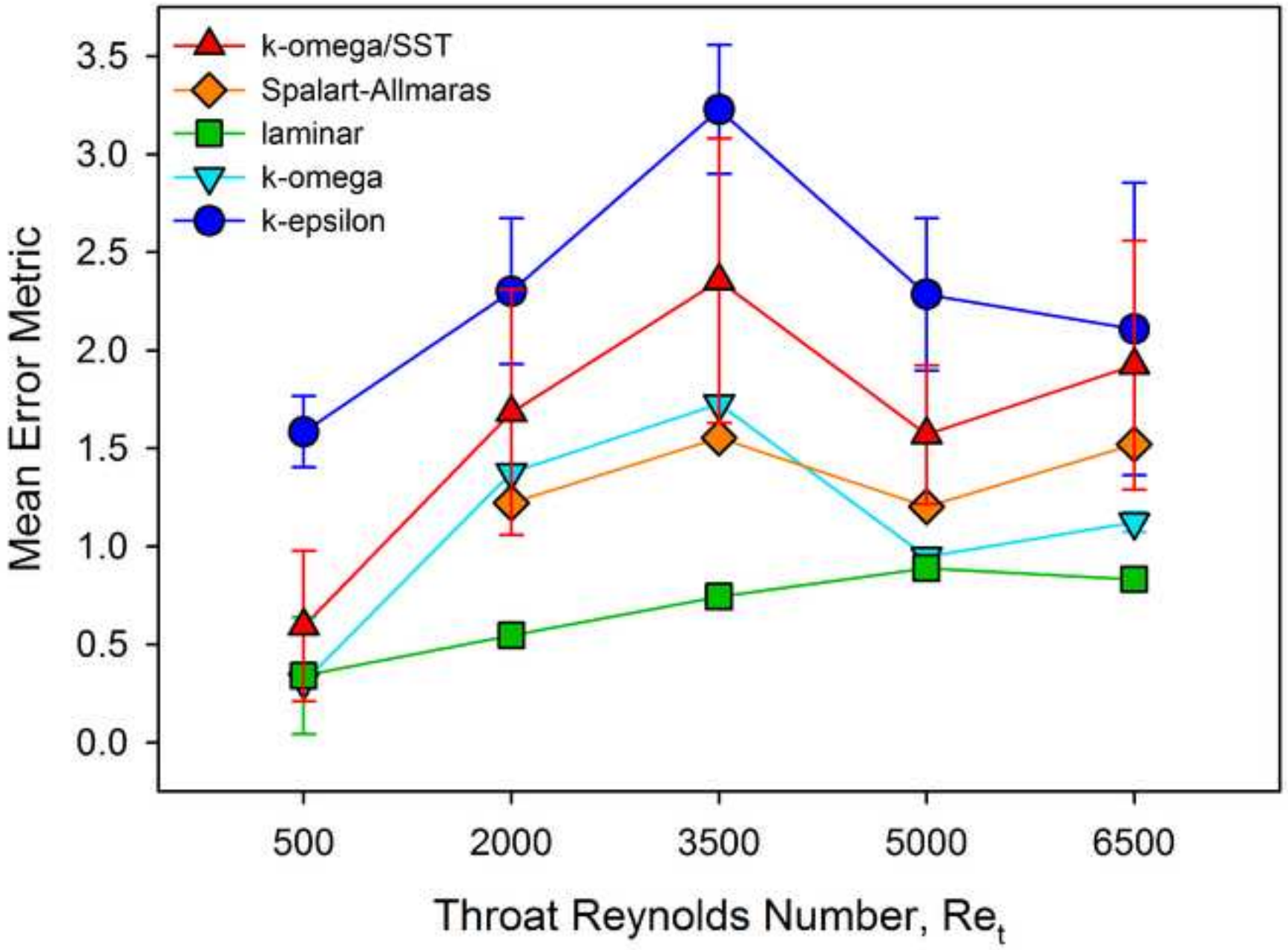

colour figure
Click here to download high resolution image

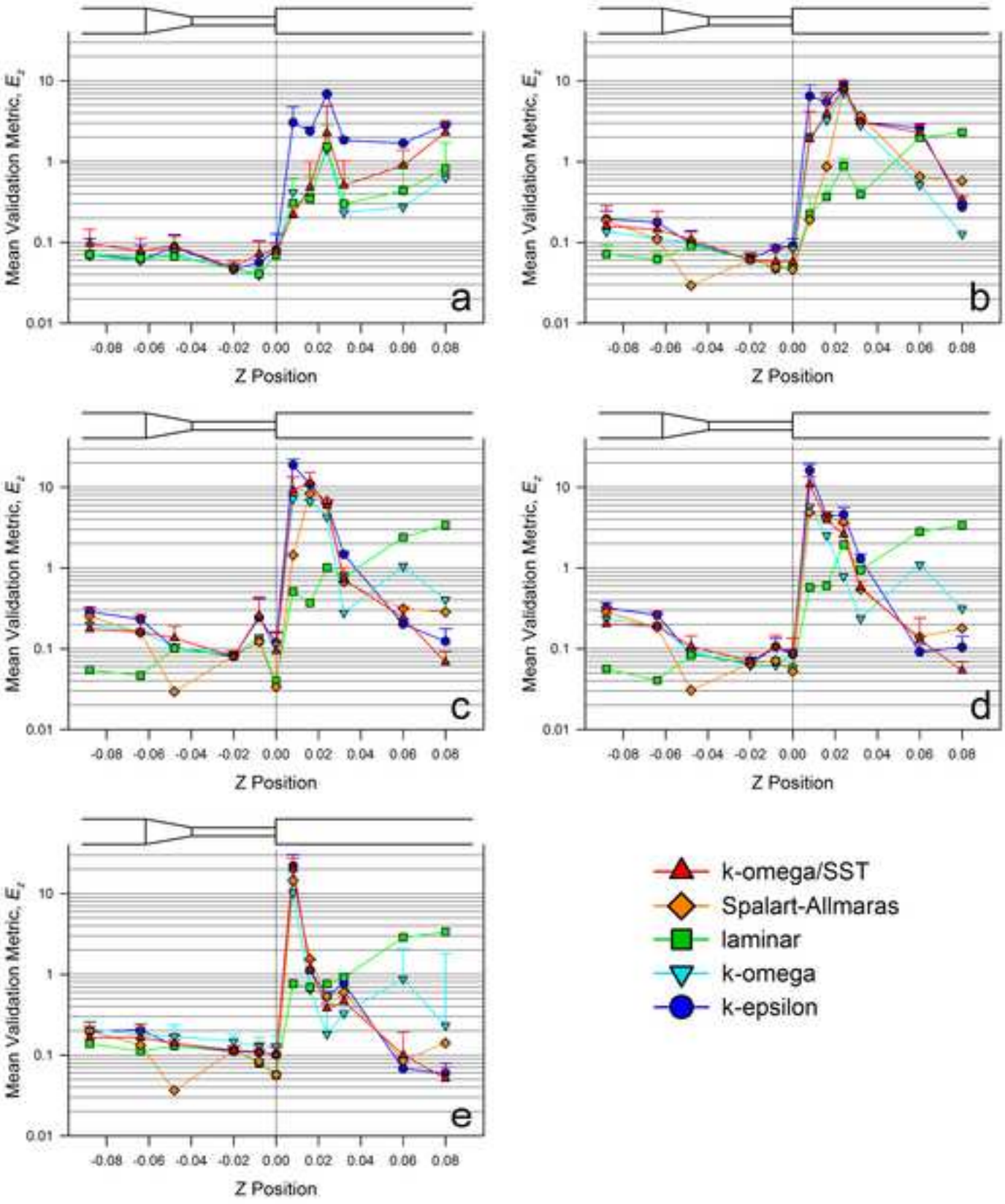

*Form for Disclosure of Potential Conflicts of Interest

Click here to download Form for Disclosure of Potential Conflicts of Interest: coi_disclosure CVET Stewart 2011.pdf